

On the Survival of Cool Clouds in the Circum-Galactic Medium

Zhihui Li^{★1}, Philip F. Hopkins¹, Jonathan Squire², Cameron Hummels¹

¹ TAPIR, Mailcode 350-17, California Institute of Technology, Pasadena, CA 91125, USA

² Department of Physics, University of Otago, 730 Cumberland St, North Dunedin, Dunedin 9016, New Zealand

ABSTRACT

We explore the survival of cool clouds in multi-phase circum-galactic media. We revisit the “cloud crushing problem” in a large survey of simulations including radiative cooling, self-shielding, self-gravity, magnetic fields, and anisotropic Braginskii conduction and viscosity (with saturation). We explore a wide range of parameters including cloud size, velocity, ambient temperature and density, as well as a variety of magnetic field configurations and cloud turbulence. We find that realistic magnetic fields and turbulence have weaker effects on cloud survival; the most important physics is radiative cooling and conduction. Self-gravity and self-shielding are important for clouds which are initially Jeans-unstable, but largely irrelevant otherwise. Non-self-gravitating, realistically magnetized clouds separate into four regimes: (1) At low column densities, clouds evaporate rapidly via conduction. (2) A “failed pressure confinement” regime, where the ambient hot gas cools too rapidly to provide pressure confinement for the cloud. (3) An “infinitely long-lived” regime, in which the cloud lifetime becomes longer than the cooling time of gas swept up in the leading bow shock, so the cloud begins to accrete and grow. (4) A “classical cloud destruction” regime, where clouds are eventually destroyed by instabilities. In the final regime, the cloud lifetime can exceed the naive cloud-crushing time owing to conduction-induced compression. However, small and/or slow-moving clouds can also evaporate more rapidly than the cloud-crushing time. We develop simple analytic models that explain the simulated cloud destruction times in this regime.

Key words: galaxies: haloes — galaxies: kinematics and dynamics — ISM: clouds — ISM: structure — galaxies: evolution

1 INTRODUCTION

The circum-galactic medium (CGM) is the diffuse, multi-phase gas surrounding a galaxy inside its virial radius and outside its disk and interstellar medium. In recent years, observations and simulations have revealed that CGM plays a significant role in galaxy evolution, in the sense that it both supplies gas for the galaxy’s star formation and recycles the energy and metals produced by stellar and AGN feedback (Tumlinson et al. 2017).

Over the past twenty years, direct observations have revealed the complex multi-phase structure in the CGM, in its ionization structure and dynamics. It is customary to classify the CGM gas into three components in different physical states (Cen 2013), namely: (a) the cool gas phase ($T < 10^5$ K), mainly composed of neutral hydrogen and low ionization-potential ions like Mg II, Si II and C II (e.g., Churchill et al. 1996; Chen et al. 1998; Steidel et al. 2010; Prochaska et al. 2014; Johnson et al. 2017); (b) the warm-hot gas phase ($T \sim 10^5 - 10^6$ K), specifically the high ionization-potential ions like C III, C IV, O VI, and Ne VIII (e.g., Stocke et al. 2006; Savage et al. 2011; Werk et al. 2014); (c) the hot gas phase ($T > 10^6$ K), consisting even more highly ionized species, like O VII and O VIII (e.g., Richter et al. 2008; Yao et al. 2010). Different ions in different physical states also display varied kinematics, resulting in a variety of absorption line profiles (Werk et al. 2016).

The existence of multi-phase gas raises fundamental questions about how the “cool” phases can be maintained. While the CGM can be thermally unstable, it is well-known from ideal-hydrodynamic simulations that a cool cloud moving through a hot medium at any appreciable velocity will be rapidly “shredded” and destroyed (mixed into the hot medium) by a combination of shocks, Rayleigh-Taylor, Kelvin-Helmholtz, and related instabilities (McKee & Cowie 1975). If clouds are “ejected” from the galaxy directly in a cool phase of galactic outflows, or form “in-situ” in outflow cooling shocks/shells, they are expected to have large (super-sonic) relative velocities to the ambient medium (Thompson et al. 2016). Even if they form in-situ in a thermally-unstable hydrostatic CGM

“halo” of hot gas around the galaxy, they are buoyantly unstable and will “sink” at trans-sonic velocities (McCourt et al. 2018).

The simple formulation of this problem – namely the survival of a cold cloud moving through a hot ambient medium – is the classical “cloud crushing” problem, and has been studied for several decades in the context of the interstellar medium (ISM), particularly for the case of giant molecular clouds (GMC) being hit by supernova shocks (e.g., Cowie & McKee 1977a; McKee & Cowie 1977; Klein et al. 1994). However, in the CGM, the dominant physics and their effects are expected to be very different from those in the ISM. For example, GMCs are marginally self-gravitating, highly supersonically-turbulent (turbulent Mach numbers $\sim 10 - 100$), molecular and self-shielding¹ (temperatures $\sim 10 - 1000$ K, column densities $\gtrsim 100 M_{\odot} \text{pc}^{-2} \sim 10^{22} \text{cm}^{-2}$), with ratios of thermal-to-magnetic pressure much less than one (plasma $\beta \ll 1$), and extremely short ion/electron mean-free-paths (negligible conduction/viscosity). CGM clouds, on the other hand, are generally not self-gravitating or Jeans-unstable, are ionized or atomic (non-molecular, non-self-shielded, with temperatures $\gtrsim 10^4$ K), exhibit weakly sub-sonic or (at most) trans-sonic turbulence (turbulent Mach numbers $\lesssim 1$), and have dynamically negligible magnetic field strengths ($\beta \gg 1$). Further, given their lower densities and higher temperatures, such clouds can be comparable in size to the mean-free-paths of hot electrons in the ambient medium, meaning that conduction and viscosity could be extremely important. Moreover, those conduction/viscosity effects will be very anisotropic, given the small ratio of the particles’ gyro radii to the system size, and could easily be in regimes where standard classical results break down.

All of this means that it is unclear how much, if any, intuition can be “borrowed” from the historical cloud-crushing studies in the ISM. As a result, there has been a recent resurgence of work on this idealized cloud-crushing problem but in the CGM context (e.g., Scannapieco & Brüggén 2015; Brüggén & Scannapieco

¹ By “self-shielding” we mean the cloud column density is high enough to absorb all the incoming ionizing photons from the meta-galactic UV background and shield the inner neutral gas from being ionized.

[★] E-mail: zhihui@caltech.edu

Table 1. Definitions of variables used in this paper

x_h	value of quantity x in the hot, ambient medium
x_{cl}	value of quantity x in the cool cloud
t_{cool}	cooling time $= (3/2)k_B T/n\Lambda$
Λ	cooling function
κ_{cond}	conduction coefficient (see Eq. 9)
ν_{visc}	viscosity coefficient (see Eq. 11)
$\ln \Lambda_D$	Coulomb logarithm ($\Lambda_D \sim n_e \lambda_D^3$)
n_e	electron number density
β	plasma $\beta \equiv P_{therm}/P_B$
P_{therm}	thermal pressure $= nk_B T$
P_B	magnetic pressure $= \mathbf{B} ^2/8\pi$
χ	density contrast n_{cl}/n_h ($= T_h/T_{cl}$, in equilibrium)
c_s	thermal sound speed
\mathcal{M}_h	initial Mach number of the hot medium $\equiv v_{cl}/c_{s,h}$
t_{cc}	classical cloud-crushing time $\equiv \chi^{1/2} R_{cl}/v_{cl}$
$t_{life, pred}$	predicted cloud lifetime from power-law fit
$t_{life, sim}$	simulated cloud lifetime
P_{ram}	ram pressure of the ambient medium $= \mu m_p n_h v_{cl}^2$

2016; Liang et al. 2016; Armillotta et al. 2017; Liang & Remming 2018; Gronke & Oh 2018, 2019; Sparre et al. 2019). However, given the more recent nature of these studies and the computational expense of simulations including all of the physics above, this work has generally been limited in one of two ways: either (1) neglecting key physics (e.g., ignoring radiative cooling, magnetic fields, anisotropic conduction/viscosity, saturation effects, or considering only two-dimensional cases), or (2) considering only a very limited parameter space (i.e., a couple of example clouds). In this paper, we therefore seek to build an analytical picture on the insights of these recent works by surveying a large parameter space of relevance to CGM clouds (e.g., of cloud sizes, column densities, and velocities, as well as ambient temperatures, densities, and magnetic field properties). We include radiative cooling, magnetic fields, and fully-anisotropic conduction and viscosity, as well as self-shielding and self-gravity, in three-dimensional high-resolution numerical simulations.

The structure of this paper is as follows. We describe the relevant physics equations, the simulation code and initial conditions, and the range of parameters surveyed, in § 2. Using our suite of simulations and analytic scalings, we then isolate various parameter regimes which give rise to *qualitatively* different behaviors in § 3. We focus on the “classical cloud destruction” regime in § 3.5: there we parameterize the dependence of the cloud lifetime on the different physical parameters described above, and discuss the effects of different physics. We summarize and conclude in § 4.

2 METHODS

2.1 Overview & Equations Solved

We wish to study the problem of a cloud moving through the ambient CGM. Within the cloud (ignoring, for now, the boundary and shock layer with the hot medium), ideal MHD should be a good approximation but the cooling times are short compared to other macroscopic timescales ($t_{cool} \sim 6 \times 10^{-5}$ Myr), so we expect clouds to be approximately isothermal at $\sim 10^4$ K (if they are not self-shielding, in which case they might be colder). In the hot medium, on the other hand, radiative cooling is usually negligible over the timescales we consider, as is self-gravity, but the deflection lengths (mean free paths) of the electrons and ions are not negligible. Because the electron and ion gyro-radii are vastly smaller than all other scales in the system, the system can be reasonably described by including appropriate, anisotropic conductive and viscous diffu-

sion coefficients (“Braginskii” conduction and viscosity; Braginskii 1965), which can provide a reasonable description of the kinetic physics at play (see e.g., discussion in Squire et al. 2019). Indeed, for the regimes considered, transport coefficients perpendicular to the magnetic field are suppressed by factors of $\sim 10^{-8}$ compared to the parallel coefficients. Given the large ionization fractions – $f_{ion} \sim 0.01 - 1$ inside the cloud, and $f_{ion} \approx 1$ outside it – we can safely neglect the effect of ambipolar diffusion, the Hall effect, and Ohmic resistivity on the evolution of the magnetic field.

The system of fluid equations we solve is therefore given by:

$$\frac{\partial \rho}{\partial t} + \nabla \cdot (\rho \mathbf{v}) = 0 \quad (1)$$

$$\frac{\partial \mathbf{v}}{\partial t} + (\mathbf{v} \cdot \nabla) \mathbf{v} = \frac{1}{\rho} \nabla \cdot \mathbf{S} - \nabla \Phi \quad (2)$$

$$\frac{\partial e}{\partial t} + \nabla \cdot (e \mathbf{v}) = \nabla \cdot (\mathbf{S} \cdot \mathbf{v} + \mathbf{K} \cdot \nabla T) - \rho \mathbf{v} \cdot \nabla \Phi - n^2 \Lambda \quad (3)$$

$$\frac{\partial \mathbf{B}}{\partial t} = \nabla \times (\mathbf{v} \times \mathbf{B}) \quad (4)$$

$$\nabla^2 \Phi = 4\pi G \rho \quad (5)$$

$$\mathbf{S} \equiv \left(P + \frac{\mathbf{B} \cdot \mathbf{B}}{2} \right) \mathbf{I} - \mathbf{B} \otimes \mathbf{B} - \mathbf{\Pi} \quad (6)$$

$$e \equiv \frac{1}{(\gamma - 1)} P + \frac{1}{2} \rho \mathbf{v} \cdot \mathbf{v} + \frac{\mathbf{B} \cdot \mathbf{B}}{2} \quad (7)$$

These are the usual continuity, momentum, energy, induction, Poisson (self-gravity) equations, for the gas mass density ρ , velocity \mathbf{v} , energy e , gravitational potential ϕ , and magnetic field \mathbf{B}^2 . Here \mathbf{S} is the stress tensor, with $P = nk_B T$ the usual isotropic (thermal) pressure (T the temperature and $n = \rho/\mu$ the particle number density, with local adiabatic index $\gamma = 5/3$). The conductivity (\mathbf{K}) and the viscous part of the stress tensor ($\mathbf{\Pi}$) are given by Spitzer & Härm (1953) and Braginskii (1965) as:

$$\mathbf{K} \equiv \kappa_{cond} \hat{B} \otimes \hat{B} \quad (8)$$

$$\kappa_{cond} = \frac{0.96 f_i (k_B T)^{5/2} k_B}{m_e^{1/2} e^4 \ln \Lambda_D} (1 + 4.2 \ell_e / \ell_T)^{-1} \quad (9)$$

$$\mathbf{\Pi} \equiv 3 \nu_{visc} \left(\hat{B} \otimes \hat{B} - \frac{1}{3} \mathbf{I} \right) \left[\left(\hat{B} \otimes \hat{B} - \frac{1}{3} \mathbf{I} \right) : (\nabla \otimes \mathbf{v}) \right] \quad (10)$$

$$\nu_{visc} = \frac{0.406 f_i m_i^{1/2} (k_B T)^{5/2}}{(Z_i e)^4 \ln \Lambda_D} (1 + 4.2 \ell_i / \ell_v)^{-1} \quad (11)$$

where \otimes denotes the outer product; \mathbf{I} is the identity matrix; “:” denotes the double-dot-product ($\mathbf{A} : \mathbf{B} \equiv \text{Trace}(\mathbf{A} \cdot \mathbf{B})$); $\ln \Lambda_D \approx 37.8$ from Sarazin (1988); m_e , e , m_i , $Z_i e = e$ are the electron mass and charge and ion mass and charge; f_i the ionized fraction (calculated self-consistently in our cooling routines); k_B the Boltzmann constant; $\ell_e \approx 0.73 (k_B T)^2 / (n_e e^4 \ln \Lambda_D)$ is the electron mean-free path and $\ell_T = T/|\nabla T|$ the temperature gradient scale length (ℓ_i and $\ell_v = |\mathbf{v}|/|\nabla \otimes \mathbf{v}|$ are the ion mean-free path and velocity gradient scale length). These additional terms account for saturation of κ or ν , although, due to the current uncertainty in the relevant physics, they neglect the effect of plasma “micro-instabilities,” which can act to limit the flux further in the high- β regime (e.g., Kunz et al. 2014; Komarov et al. 2016). At a sharp discontinuity – for example, the contact discontinuity at the edge of the cloud – the form of Eq. (9) ensures the conductive flux takes the saturated form from Cowie & McKee (1977a): $q_{sat} \approx 0.4 (2k_B T / \pi m_e)^{1/2} n_e k_B T \cos \theta \hat{B}$ (where θ is the angle between \mathbf{B} and ∇T). Note, however, that by solving a single set of fluid equations we are assuming that ions and

² To maintain $\nabla \cdot \mathbf{B} = 0$, we adopt the divergence cleaning scheme proposed in Dedner et al. (2002) and the constrained gradient scheme in Hopkins (2016).

Table 2. Parameters varied

Name	Description	Values considered
L_{cl}	initial cloud diameter ($=2R_{\text{cl}}$)	0.01, 0.1, 1, 10, 100, 1000 pc
v_{cl}	initial cloud velocity	10, 100, 1000 km s $^{-1}$
T_{h}	ambient temperature	$10^5, 10^6, 10^7$ K
n_{h}	ambient density	$10^{-4}, 10^{-3}, 10^{-2}, 10^{-1}$ cm $^{-3}$

The description and parameter space of the main physical parameters varied in this paper.

electrons maintain similar temperatures, despite the species having different conductive heat fluxes. Finally, $\Lambda = \Lambda(T, n, Z, I_{\nu}, \dots)$ represents cooling *and* heating (so it can have either sign) via additional processes such as radiation, cosmic rays, dust collisions and photoelectric processes, etc (details below).

2.2 Simulation Code

We solve the equations (1)-(11) in the code GIZMO (Hopkins 2015)³, which uses a Lagrangian mesh-free finite-volume Godunov method, in its meshless finite-volume (finite-element) “MFV” mode. We have also compared simulations using GIZMO with its meshless finite-mass, or fixed-grid finite volume solvers, to verify that the choice of hydrodynamic solver in GIZMO has only small effects on our results. Hopkins (2015), Hopkins & Raives (2016), and Hopkins (2016, 2017) present details of these methods and extensive tests of their accuracy and convergence in good agreement with state-of-the-art grid codes (e.g., ATHENA). In particular the MFV method is manifestly conservative of mass, momentum, and energy, with sharp shock-capturing and accurate treatment of fluid-mixing instabilities (e.g., Kelvin-Helmholtz (KH) and Rayleigh-Taylor (RT) instabilities), and correctly captures MHD phenomena including the magneto-rotational instability (MRI), magnetic jet launching in disks, magnetic fluid-mixing instabilities, and sub-sonic and super-sonic MHD turbulent dynamos. In Hopkins (2017), we show that the numerical implementation of the anisotropic diffusion operators (**K** and **II**) is accurate, able to handle arbitrarily large anisotropies, converges comparably to higher-order fixed-grid codes, and is able to correctly capture complicated non-linear instabilities sourced by anisotropic diffusion such as the magneto-thermal and heat-flux buoyancy instabilities; this has also been tested in fully non-linear simulations of galaxy and star formation (Su et al. 2017). GIZMO also includes full self-gravity (ϕ) using an improved version of the Tree-PM solver from GADGET-3 (Springel 2005), with fully-adaptive and conservative gravitational force softening (so hydrodynamic and gravitational force resolution is self-consistently matched) following Price & Monaghan (2007). Finally, GIZMO includes a detailed, fully-implicit solver for radiative heating and cooling (Λ). We use the cooling physics from the cosmological FIRE galaxy simulations, with all details given in Appendix B of Hopkins et al. (2018): cooling is tracked self-consistently from $10 - 10^{10}$ K, including free-free, photo-ionization/recombination, Compton, photoelectric & dust collisional, cosmic ray, molecular, and metal-line & fine-structure processes (tabulated from CLOUDY; Ferland et al. 1998) from each of 11 species, accounting for photo-heating by a meta-galactic UV background (using the $z = 0$ value from Faucher-Giguère et al. 2009), with self-shielding (as in Rahmati et al. 2013) and optically-thick cooling. Additional details are provided in Hopkins et al. (2018); the cooling physics have been used extensively in simulations of star and galaxy formation in the FIRE project. Ionization states are calculated self-consistently accounting for both collisional and photo-ionization.

³ A public version of this code is available at <http://www.tapir.caltech.edu/~phopkins/Site/GIZMO.html>.

2.3 Initial Conditions & “Default” Problem Setup

Our simulations follow a standard “cloud crushing” problem setup, always in three dimensions. For simplicity, a spherical cloud of radius R_{cl} and mean density $n_{\text{cl}} \equiv M_{\text{cl}}/(4\pi/3 R_{\text{cl}}^3 m_p)$ is initialized at an equilibrium temperature $T_{\text{cl}} \sim 10^4$ K (with heating and cooling from the meta-galactic UV background), in pressure equilibrium with a homogeneous box filled with gas at electron density $n_e = n_{\text{h}}$, temperature T_{h} , and relative velocity $\mathbf{v} = v_{\text{cl}} \hat{y}$ to the cloud (we relax the cloud before turning on velocities to ensure equilibrium temperature and pressure⁴). The system is contained in a periodic box with size-length $10R_{\text{cl}}$ in the \hat{x} and \hat{z} directions and $20R_{\text{cl}}$ in the \hat{y} direction, with an inflow boundary on the “upwind” \hat{y} side such that the upwind portion of the box is always filled with gas at the initial ambient properties (with outflow out of the opposite \hat{y} side). The box moves with the cloud meaning that we can follow the system over long evolution times⁵, as long as the cloud does not become sufficiently elongated that it exceeds the box size. We have run simulations with box sizes up to $\sim 100R_{\text{cl}}$ in length to verify that this does not affect our conclusions. One advantage of our Lagrangian code is that it makes no difference (to machine precision) whether we assign the velocity to the cloud or ambient medium.

In our “default” simulations, the box is populated with equal-mass resolution elements with $m_i \approx 10^{-6} M_{\text{cl}}$. Because the method is Lagrangian, our mass resolution is fixed but spatial resolution is automatically adaptive with $\Delta x_i \approx 0.01 R_{\text{cl}} (n/n_{\text{cl}})^{-1/3} (m_i/10^{-6} M_{\text{cl}})^{1/3}$. In some of the simulations below we disable self-shielding⁶ and self-gravity: without self-shielding there is effectively a temperature floor of $\sim 10^4$ K set by the UV background, while with self-shielding gas can cool to ~ 10 K in principle. The default simulations initialize an intentionally weak uniform magnetic field with $\beta \equiv P_{\text{therm}}/P_B = 10^6$, oriented perpendicular to the cloud velocity vector, but we vary this below. A small subset of our simulations consider “turbulent” initial conditions, as described below. In Appendix A, we show the effects of changing resolution ($m_i \sim 10^{-7} - 10^{-3} M_{\text{cl}}$) and verify that the predicted cloud lifetimes are robust to the choice of resolution.

Table 2 lists the key physical parameters that we vary between simulations. We survey a wide range of parameters, including L_{cl} from 0.01 to 1000 pc, v_{cl} from 10 to 1000 km s $^{-1}$, T_{h} from 10^5 to 10^7 K, and n_{h} from 10^{-4} to 10^{-1} cm $^{-3}$.

2.4 Definition of Cloud “Destruction” and “Lifetime”

Although it is often obvious “by-eye” when a cloud is being “destroyed” or “mixed,” there is no obvious rigorous definition. Following one common convention in the literature, we simply define the “cloud mass” as the mass above some density threshold relative to the background. Since we consider a range of clouds with different initial density contrasts, we specifically define the mass variable $m_{\text{cl},x}$ as the mass in the box with density $\log \rho > \log \rho_{\text{h}}^0 + (x/100) (\log \rho_{\text{cl}}^0 - \log \rho_{\text{h}}^0)$, where ρ_{h}^0 and ρ_{cl}^0 are the initial ambient and cloud mean densities. So $m_{\text{cl},50}$ is the mass above a density threshold equal to $(\rho_{\text{cl}}^0 \rho_{\text{h}}^0)^{1/2}$, i.e., the geometric mean of the initial cloud and ambient medium densities. We have experimented with different values of x from $\sim 5 - 95$, as well as different functional forms for a density threshold and combined density-temperature thresholds. We find that $m_{\text{cl},50}$ defined in this manner

⁴ We confirm that the cloud expansion during the relaxation process is negligible and does not affect the subsequent cloud evolution.

⁵ Every time when the cloud material gets too close to the boundary of the box, we shift the entire box to accommodate the cloud again.

⁶ We account for self-shielding following Faucher-Giguère et al. (2015) by locally attenuating the UV background. So to disable self-shielding we simply unattenuate the UV background.

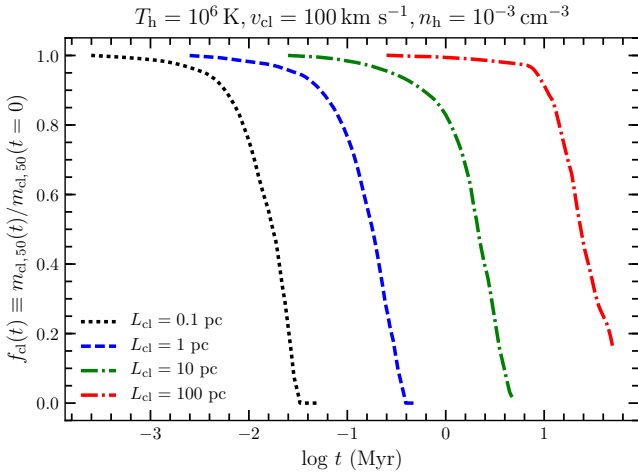


Figure 1. Time evolution of the normalized cloud masses, $f_{\text{cl}}(t)$, for four clouds with initial conditions of $T_{\text{h}} = 10^6$ K, $v_{\text{cl}} = 100$ km s $^{-1}$, $n_{\text{h}} = 10^{-3}$ cm $^{-3}$ and $L_{\text{cl}} = 0.1$ -100 pc. Here $f_{\text{cl}}(t)$ is defined as $m_{\text{cl},50}(t)/m_{\text{cl},50}(t=0)$, where $m_{\text{cl},50}$ is the cloud mass with density $\rho > (\rho_{\text{cl}}^0 \rho_{\text{h}}^0)^{1/2}$, i.e., the geometric mean of the initial cloud and ambient medium densities. These clouds “disrupt” in a well-defined manner in our simulations. We therefore define a cloud “lifetime”, t_{lifc} , as the time when the cloud mass falls below 10% of its initial value for the first time, i.e., $f_{\text{cl}}(t = t_{\text{lifc}}) \leq 0.1$.

gives the most robust estimate of the visually-identified “cloud” material, so we will adopt this by default throughout.

Figure 1 shows several examples of the cloud mass estimator, $f_{\text{cl}}(t) \equiv m_{\text{cl},50}(t)/m_{\text{cl},50}(t=0)$ (cloud mass normalized to the initial cloud mass at time $t=0$), as a function of time. We see in many of the cases discussed below that the cloud mass (mass remaining at high densities) declines steadily with time. In these cases, it is convenient to define a “lifetime” t_{lifc} of the cloud, although this is again somewhat arbitrary. We define this as the time when $f_{\text{cl}}(t = t_{\text{lifc}}) \leq 0.1$ for the first time – i.e., when the cloud mass as defined above falls below 10% of its initial value. We find this is more stable than fitting, e.g., an exponential or power-law decay timescale, because exponential or power-law decay is often not a good approximation to the simulation results. The choice of $\sim 10\%$ of the initial mass is arbitrary, but our results are qualitatively identical for choices in the range $\sim 1 - 50\%$ (above $\sim 50\%$, we find we often under-estimate the lifetimes of clouds, as they partially disrupt or evaporate but retain a long-lived “core,” and below $\sim 1 - 2\%$, resolution concerns begin to dominate).

Not all clouds decay in mass: as we will show below, some grow. For these, we can define a growth timescale as the approximate e -folding time.

3 DIFFERENT REGIMES OF DOMINANT PHYSICS

Guided by our simulation parameter survey, plus some basic analytic considerations, we now define different regimes of cloud behavior in the CGM and the most relevant physics in each.

3.1 The Smallest Clouds: Where Conduction Breaks Down

The thermal conductivity of the hot medium is defined by the transport of hot electrons, with $\kappa/k_{\text{B}} n_{\text{h}} \sim \lambda_{e,\text{h}} c_{s,e,\text{h}}$ where

$$\lambda_{e,\text{h}} \equiv 3 m_e^{1/2} (k_{\text{B}} T_e)^{3/2} c_{s,e,\text{h}} / (4\sqrt{2\pi} n_i e^4 \ln \Lambda_D) \approx 0.1 \text{ pc} \frac{T_6^2}{n_{\text{h},0.01}} \quad (12)$$

(using $\ln \Lambda_D \approx 26$ for $T_{\text{h}} \sim 10^5 - 10^6$ K) is the electron Coulomb deflection length (along the magnetic field) and $c_{s,e,\text{h}}$ is the electron isothermal sound speed ($\equiv \sqrt{k_{\text{B}} T_{\text{h}}/m_e}$) defined in the hot medium. When the hot electrons encounter a cold cloud, they are able to

penetrate to a skin depth $\lambda_{\text{skin}} = \lambda_{e,\text{h}} (n_{\text{h}}/n_{\text{cl}}) = \lambda_{e,\text{h}} (T_{\text{cl}}/T_{\text{h}})$. If $\lambda_{\text{skin}} \gtrsim R_{\text{cl}}$, then our description of heat transport (conduction) via Eq. (3) breaks down (regardless of the accounting for saturated v.s. unsaturated conduction). Using the values above, this occurs when

$$N_{\text{H}} \lesssim N_{\text{H}}^{\text{mfp}} \sim 10^{16} \text{ cm}^{-2} T_6^2 \quad (13)$$

where $T_6 \equiv T_{\text{h}}/10^6$ K, and $N_{\text{H}} \equiv R_{\text{cl}} \langle n_{\text{cl}} \rangle$ is the column density through the cloud⁷.

We therefore intentionally avoid simulating systems below this scale. However, we can estimate what will occur. In this limit, the free e^- in the hot medium effectively do not “see” the cloud: the cloud will effectively be immersed in a sea of hot e^- with number density equal to the ambient hot e^- density, which contribute a uniform volumetric Coulomb heating rate. If the cloud is ionized, this is just $\dot{e} = 0.34 n_{e,\text{h}} (c_{s,e,\text{h}}/\lambda_{\text{skin}}) k_{\text{B}} T_{\text{h}}$ (Brüggen & Scannapieco 2016), and if $T_6^{3/2} \Lambda_{\text{cl},-23} \lesssim 0.14$, then the volumetric heating rate from hot e^- is larger than the cooling rate of gas in the cloud, and they should evaporate on a timescale short compared to their sound-crossing times. This process is analysed in detail in Balbus & McKee (1982).

3.2 Self-gravity & Self-Shielding

At the other extreme, consider very large clouds. If a cloud is *initially* self-gravitating/J Jeans-unstable, i.e., has $\lambda_{\text{J}} \equiv c_{s,\text{cl}}/\sqrt{G\rho_{\text{cl}}} \ll R_{\text{cl}}$, or $R_{\text{cl}} \gtrsim 1 \text{ kpc} (n_{\text{h},0.01} T_6)^{-1/2}$, or

$$N_{\text{H}} \gtrsim N_{\text{H}}^{\text{grav}} \sim 0.5 \times 10^{22} \text{ cm}^{-2} (n_{\text{h},0.01} T_6)^{1/2} \sim 10^{22} \text{ cm}^{-2} P_{-12}^{1/2} \quad (14)$$

where $P_{-12} \equiv P_{\text{h}}/10^{-12} \text{ erg cm}^{-3}$, then (a) the gravitational force per unit area is larger than the external (confining/stripping) pressure, and (b) its collapse/free-fall time is shorter than its sound-crossing time, itself shorter than the cloud destruction time (in the absence of gravity). Figure 2 shows that in our simulations with self-gravity on, we confirm that clouds which are initially Jeans-unstable ($N_{\text{H}} > N_{\text{H}}^{\text{grav}}$; Eq. 14) indeed fragment/collapse rapidly⁸, while clouds which are initially Jeans-stable ($N_{\text{H}} < N_{\text{H}}^{\text{grav}}$) behave essentially identically whether or not self-gravity is included. Thus, self-gravity is very much a “threshold” effect: it dominates in Jeans-unstable clouds, and is irrelevant in Jeans-stable clouds (at least on the spatial/time scales we simulate). There is only a very narrow, fine-tuned, and dynamically unstable parameter space where clouds are “just barely” Jeans-stable initially and can have sub-regions “pushed into” Jeans instability by their interactions with the ambient medium (we find just one such example in our entire parameter survey, with initial $N_{\text{H}} \sim 0.8 N_{\text{H}}^{\text{grav}}$)⁹. This should not be surprising:

⁷ It is sometimes stated that the “fluid approximation” breaks down on scales small compared to λ_{skin} or even the (much larger) $\lambda_{e,\text{h}}$, but this is not necessarily correct. So long as the gyro radii of the particles remain small compared to the relevant scales, equations with a similar form to the fluid MHD equations (the “kinetic MHD” equations of Kulsrud 1983) remain valid. However, our descriptions of parallel heat and momentum transport clearly become problematic below λ_{skin} , as does the assumption that the electrons and ions remain at the same temperature.

⁸ Since we do not include star formation, we eventually stop the simulations when most of the gas in the initial cloud has collapsed to densities $> 10^5$ times larger than its initial mean density.

⁹ This is expected: 1D compression (e.g., the initial “pancaking” of the cloud as it shocks) does not strongly enhance Jeans instability. Consider an initially Jeans-stable, isothermal cloud with (pre-shock) Jeans length $\lambda_{\text{J}}^0 > R_0$ (radius $R = R_0$), compressed or “pancaked” to width $H \ll R_0$ along the short axis (retaining $R = R_0$ along the long axis). Fragmentation along the short axis requires a Jeans-like criterion $\lambda_{\text{J}}^{\text{new}} < H$, but $\lambda_{\text{J}}^{\text{new}} = c_{s,\text{cl}}/\sqrt{G\rho_{\text{cl}}^{\text{new}}} \sim H (\lambda_{\text{J}}^0/R_0) (R_0/H)^{1/2} \gg H$. Along the long-axis, fragmentation must be treated two-dimensionally, and requires $\lambda_{\text{J}}^{2D} < R_0$

the same behavior has been repeatedly demonstrated for clouds in the ISM (see e.g., Mouschovias 1976a,b; Li et al. 2014; Federrath & Banerjee 2015; Körtgen et al. 2019).

Likewise, if the cloud can *initially* self-shield to molecular or fine-structure metal-line cooling to temperatures $T \sim 10 - 100\text{ K} \ll 10^4\text{ K}$, it will cool to those temperatures very quickly, which will remove its internal pressure support and render it immediately Jeans-unstable (even more so, given the rapid compression by the ambient medium which would follow). This is well-studied in the ISM context and requires a surface density $\gtrsim 10 M_\odot \text{pc}^{-2} (Z_\odot/Z)$ (see Robertson & Kravtsov 2008; Krumholz & Gnedin 2011, for extended discussion), or a column density

$$N_{\text{H}} \gtrsim N_{\text{H}}^{\text{shield}} \sim 1.5 \times 10^{22} \text{ cm}^{-2} Z_{0.1}^{-1} \quad (15)$$

where $Z_{0.1} \equiv Z/0.1 Z_\odot$. Like with self-gravity, we find this is a sharp “threshold” effect, not surprising since the self-shielding attenuation ($\propto e^{-\tau}$) is an extremely strong function of the N_{H} , which can vary by orders of magnitude. Usually, self-shielded clouds ($N_{\text{H}} > N_{\text{H}}^{\text{shield}}$, Eq. 15) are already self-gravitating, but it is largely irrelevant which occurs “first.” A self-shielded (but initially Jeans-stable) cloud rapidly becomes Jeans-unstable, while a Jeans-unstable (but non-shielded) cloud collapses isothermally (at $\sim 10^4\text{ K}$) until it becomes self-shielded, then collapses more rapidly (see Robertson & Kravtsov 2008; Orr et al. 2018). Because the criterion here is a simple column-density threshold, it is also obvious that 1D compression of the cloud does not strongly alter its self-shielding. For the sake of completeness and testing our theory of cloud destruction, we have re-run all our simulations *without* self-gravity and self-shielding, so we can see whether and “how fast” they would be destroyed in the absence of these physics in our analysis below, but we stress that this is purely a counter-factual exercise.

3.3 Rapid Cooling of the Hot Medium: Failure of Pressure Confinement

If the hot gas cools faster than the time it takes to cross/envelop the cloud, it cannot maintain meaningful pressure confinement. Even if we add some global (spatially-uniform) heating rate per unit volume or heat conduction in the hot medium, such that the ambient gas *equilibrium* temperature remains fixed at the “target” temperature, in this limit the hot gas is still thermally unstable and it cannot respond to perturbations of the cloud shape or expansion of the cloud, so the cloud will behave as if it is in an essentially pressure-free medium. This occurs when $t_{\text{cool,h}} \lesssim t_{\text{cross}} \sim R_{\text{cl}}/v_{\text{cl}}$ (or $R_{\text{cl}}/c_{\text{s,cl}}$ if $v_{\text{cl}} \lesssim c_{\text{s,cl}}$), giving:

$$N_{\text{H}} \gtrsim N_{\text{H}}^{\text{confine}} \sim 0.5 \times 10^{22} \text{ cm}^{-2} T_6^2 v_{100} \Lambda_{\text{h},-23}^{-1} \quad (16)$$

where $v_{100} \equiv v_{\text{cl}}/100 \text{ km s}^{-1}$ and $\Lambda_{\text{h},x} \equiv \Lambda(n_{\text{h}}, T_{\text{h}}, Z_{\text{h}})/10^x \text{ erg cm}^3$. For $T_{\text{h}} \gtrsim 10^6\text{ K}$, this requires larger column densities than would already be self-gravitating or self-shielding, so this parameter regime becomes irrelevant. However, when the hot medium is cooler than $\sim 10^6\text{ K}$, cooling becomes much more efficient, and the required N_{H} for this regime drops rapidly (to $\gtrsim 10^{18} \text{ cm}^{-2}$ at $T_{\text{h}} \sim 10^5\text{ K}$). In the CGM, this naturally coincides with the virial temperatures below which “hot halos” that can maintain a stable virial shock and quasi-hydrostatic pressure-supported gas halo cease to exist.

In Figure 3 and 4, we confirm in our simulations that clouds with $N_{\text{H}} \gtrsim N_{\text{H}}^{\text{confine}}$ (Eq. 16) indeed behave as if there is negligible confining pressure. As shown in the lower right panel of Figure 4, they expand into the ambient, low-pressure medium, which does cause the cloud density to decrease, but ambient gas cooling/accretion also causes the cloud mass to grow, so this is clearly

where $\lambda_{\text{J}}^{2D} \equiv c_s^2/(\pi G \Sigma_{\text{cloud}}) \sim R_0 (\lambda_{\text{J}}^0/R_0)^2 \gg R_0$. So an initially Jeans-stable cloud remains stable.

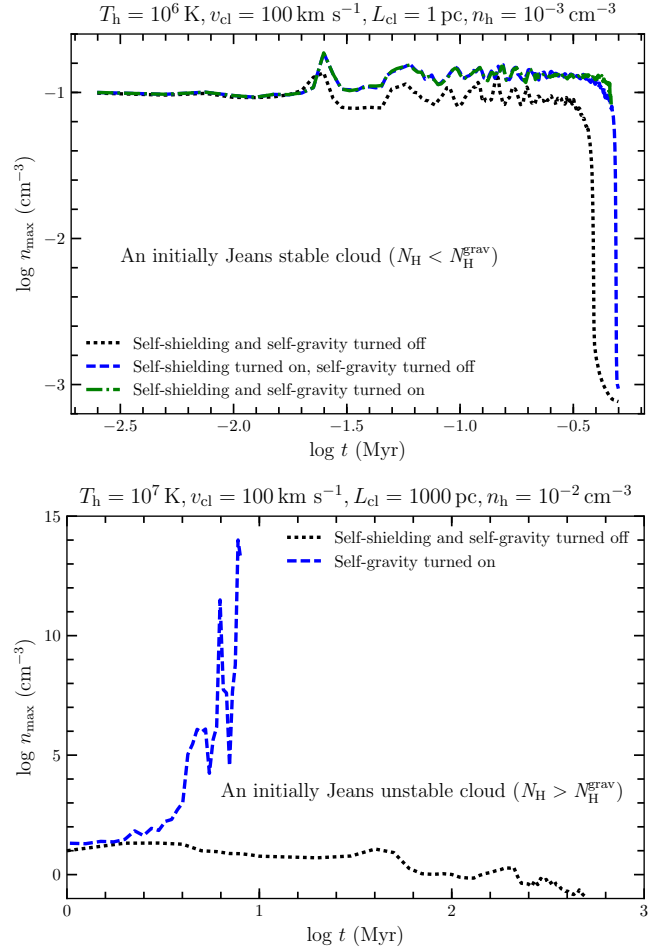


Figure 2. Time evolution of the maximum density (n_{max}) in a cloud for two representative cases. *Upper:* If $N_{\text{H}} \lesssim N_{\text{H}}^{\text{grav}}$ (Eq. 14), i.e., the cloud is initially Jeans-stable, then turning on or off self-gravity or self-shielding makes little difference. *Lower:* If $N_{\text{H}} \gtrsim N_{\text{H}}^{\text{grav}}$ (the cloud is initially Jeans-unstable), turning on self-gravity leads to cloud collapse (n_{max} runs away) in a free-fall time, as expected.

distinct from classical cloud “destruction”. If Eq. (16) is satisfied, the failure of pressure confinement occurs with or without the addition of an artificial spatially-uniform heating rate Q (such that the heating+cooling rate per unit volume is $\dot{\epsilon} = Q - n^2 \Lambda$), with Q chosen so the hot gas evolved in isolation (no cold cloud) remains exactly at its initial temperature. While not surprising, this is important for application of our conclusions in the CGM, especially around dwarf galaxies, which are in the “cold mode” of accretion without “hot halos” (Kereš & Hernquist 2009). In that regime, cold clouds from e.g., galactic winds may well have $N_{\text{H}} \gtrsim N_{\text{H}}^{\text{confine}}$, and thus could behave as if they are expanding into vacuum.

3.4 Clouds Grow: Accreting Ambient Hot Gas

As discussed in recent work by e.g., Gronke & Oh (2018, 2019), if clouds avoid destruction for a time longer than the cooling time of swept-up material, the front of the hot material entrained by the cloud (and mixing with the denser, cooler, cloud material) cools rapidly and effectively gets “accreted” onto the cloud. We can crudely estimate when this occurs by comparing our estimated cloud destruction time via “shredding” (in the absence of cooling), $t_{\text{life,pred}} \sim 10 t_{\text{cc}} \tilde{f}$ (defined in § 3.5 below) to the cooling time of the hot medium, $t_{\text{cool,h}}$. This gives:

$$N_{\text{H}} \gtrsim N_{\text{H}}^{\text{grow}} \sim 2 \times 10^{20} \text{ cm}^{-2} T_6^{3/2} v_{100} \tilde{f}^{-1} \Lambda_{\text{h},-23}^{-1} \quad (17)$$

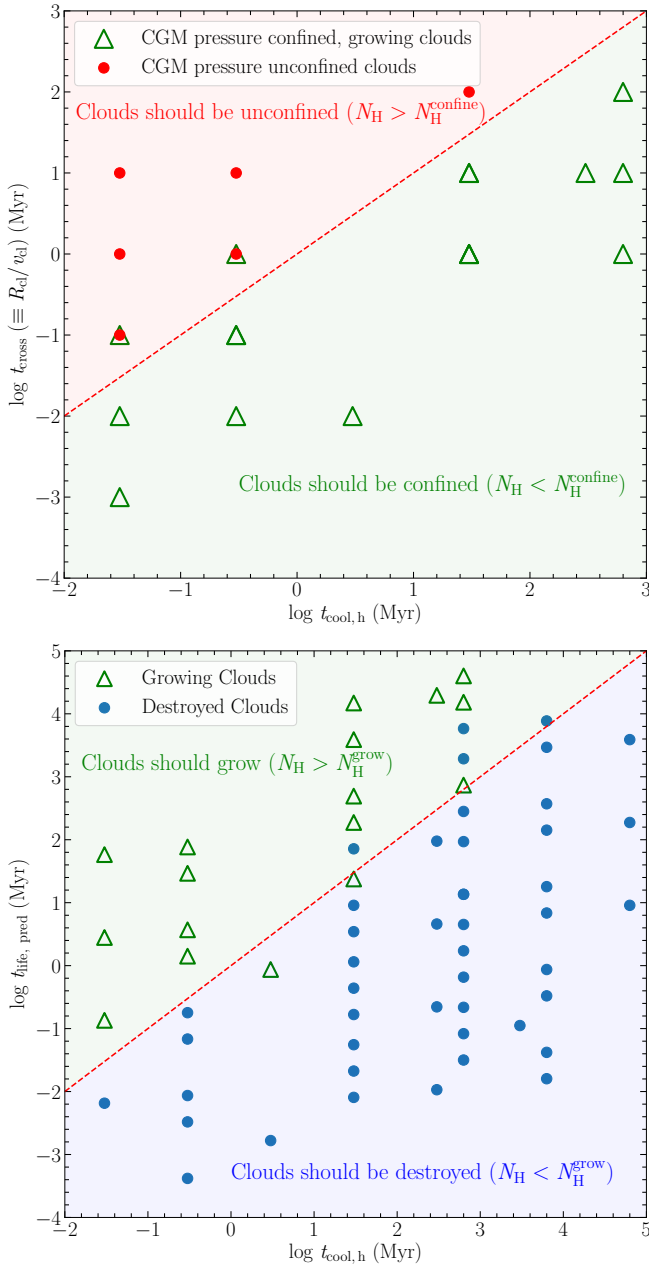


Figure 3. Simulation tests of the criteria for separating different cloud behaviors discussed in § 3.3 and § 3.4. *Upper:* Cooling time of ambient hot gas ($t_{\text{cool,h}}$) v.s. crossing time of that gas over the cloud (t_{cross}). When cooling is faster than cloud velocity/sound crossing times, the clouds cannot be meaningfully pressure-confined and simply expand (neglecting self-gravity). The green triangles denote simulations used to check this directly, which confirm the validity of the simple analytic criteria for this behavior in Eq. (16). *Lower:* Same, but comparing $t_{\text{cool,h}}$ to the cloud “destruction time” in the limit where cooling is *not* important ($t_{\text{life,pred}}$, given in § 3.5, Eq. 19). When cooling of the hot gas in the cloud front is faster than cloud disruption, the cloud accretes and grows: simulations confirm the simple analytic criterion derived in Eq. (17).

(The material in the front has been heated modestly by compression and/or shocks, but also increased in density, and rapid conduction suppresses temperature variations; thus for the conditions simulated here the cooling time of the front material is order-unity similar to the cooling time in the ambient gas). For the range of parameters of interest in the CGM, this *almost always* occurs at lower N_{H} compared to the “failure of pressure confinement” above. So if a cloud “begins” life in-between ($N_{\text{H}}^{\text{grow}} \lesssim N_{\text{H}} \lesssim N_{\text{H}}^{\text{confine}}$), it will grow until

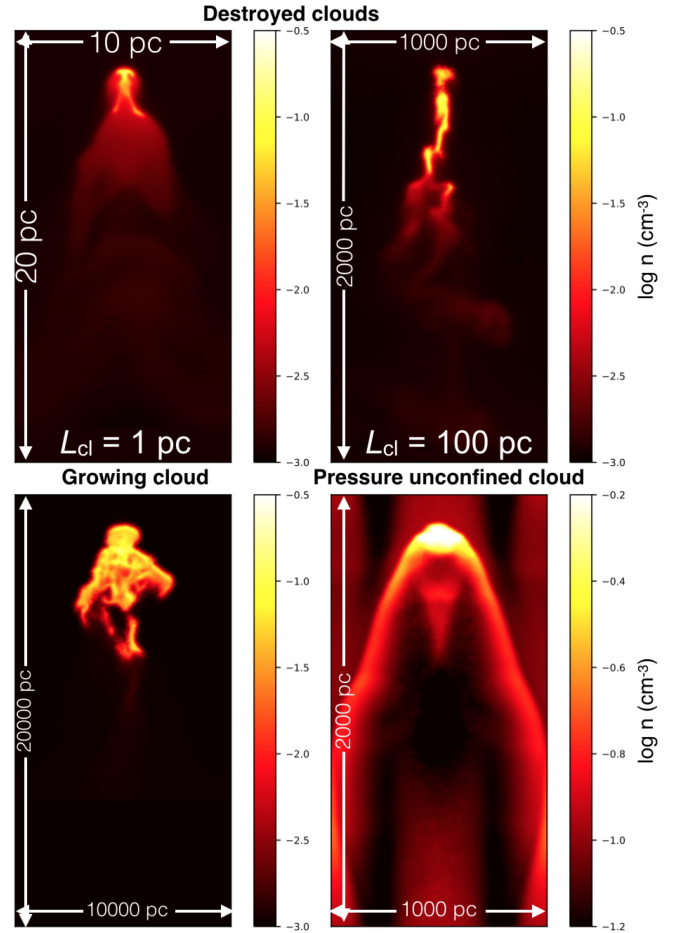


Figure 4. *Upper:* Sliced density maps of two clouds in the “classical cloud destruction” regime with initial conditions of $T_{\text{h}} = 10^6$ K, $v_{\text{cl}} = 100$ km s $^{-1}$, $n_{\text{h}} = 10^{-3}$ cm $^{-3}$, $L_{\text{cl}} = 1$ and 100 pc, respectively. *Lower left:* Sliced density map of a “growing” cloud ($N_{\text{H}} \gtrsim N_{\text{H}}^{\text{grow}}$, with $T_{\text{h}} = 10^6$ K, $v_{\text{cl}} = 100$ km s $^{-1}$, $n_{\text{h}} = 10^{-3}$ cm $^{-3}$, $L_{\text{cl}} = 1000$ pc). *Lower right:* Sliced density map of a “pressure unconfined” cloud ($N_{\text{H}} \gtrsim N_{\text{H}}^{\text{confine}}$, with $T_{\text{h}} = 10^5$ K, $v_{\text{cl}} = 100$ km s $^{-1}$, $n_{\text{h}} = 10^{-1}$ cm $^{-3}$, $L_{\text{cl}} = 100$ pc).

it reaches that larger N_{H} threshold, at which point it will continue to “sweep up” any gas in its path, but also expand in the “backward” direction as the gas cools around it. Note that, however, if the cloud increases its N_{H} (mass) by an order-unity factor, momentum conservation requires it decelerate by a similar factor. So the cloud will slow down and stop, which in turn decreases v_{100} , making it even more above-threshold to survive. So we end up with essentially static, long-lived clouds in this limit.

Note that [Gronke & Oh \(2019\)](#) derive a criterion for “cloud growth” that is slightly different from ours. They start from the same principle, comparing cloud lifetimes and cooling time in the mixing layer/front, but assume the cloud lifetime is t_{cc} and the cooling time of the ambient hot gas is $t_{\text{cool,h}}/\chi$ (this arises from assuming the “near-cloud” hot gas has geometric-mean temperature and density between cloud and ambient medium, and neglecting the dependence of Λ on T). Accounting for both efficient conduction and rapid “sweeping” of the hot gas past the cloud, we find that simply using $t_{\text{cool,h}}$ for the ambient gas, together with our more accurate cloud lifetime estimates, provides a more accurate and robust criterion for distinguishing between “growing” and “destroyed” cloud cases. This is especially true at high ambient temperatures ($T_{\text{h}} \gtrsim 10^6$ K), as can be seen in the lower panel of Figure 3. One possible explanation is that efficient conduction heats up the gas in the front and makes it difficult for a mixing layer at intermediate temperature to

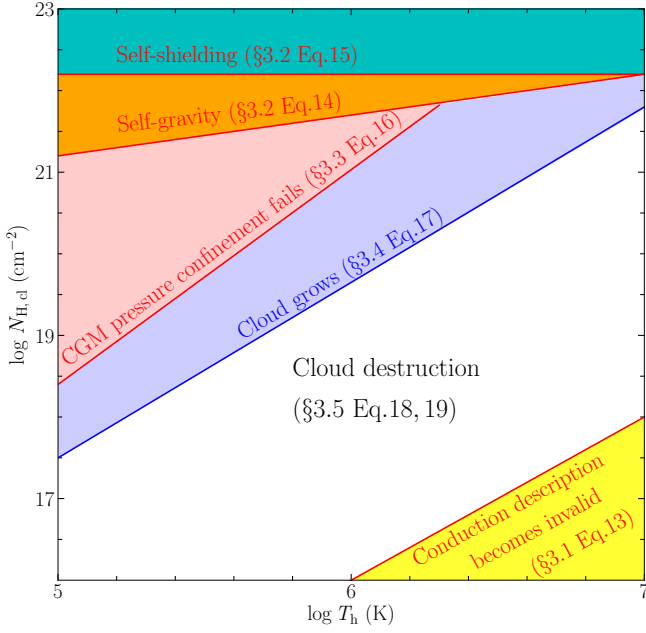


Figure 5. The cloud column density ($N_{\text{H,cl}}$) v.s. the temperature of the ambient medium (T_{h}). Different regimes of dominant physics are shown: (1) The “conduction description fails” regime (§3.1, Eq. 13, shown in yellow); (2) The “self-shielding and self-gravity dominate” regime (§3.2, Eq. 14, 15, shown in green and orange); (3) The “CGM pressure confinement fails” regime (§3.3, Eq. 16, shown in pink); (4) The “cloud grows” regime (§3.4, Eq. 17, shown in blue); (5) The “classical cloud destruction” regime (§3.5, Eq. 18, shown in white). Typical values of certain parameters have been adopted ($v_{\text{cl}} = 100 \text{ km s}^{-1}$, $n_{\text{h}} = 10^{-2} \text{ cm}^{-3}$, $\tilde{f} = 1$).

exist. This effect is shown in the density maps we present in §3.5.3, where the cloud with conduction has sharper edges, indicating a sharper density and temperature contrast. Understanding the cause of this discrepancy in more detail will be left to future work.

3.5 In-Between: Classical Cloud “Destruction” (Shredding)

If we exclude all of the regimes above, i.e., consider only clouds with

$$N_{\text{H}}^{\text{mfp}} \ll N_{\text{H}} \ll \min \left\{ N_{\text{H}}^{\text{grow}}, N_{\text{H}}^{\text{confine}}, N_{\text{H}}^{\text{shield}}, N_{\text{H}}^{\text{grav}} \right\} \quad (18)$$

then we find that all the clouds we simulate are eventually destroyed/dissolved. The boundaries of this parameter space (where clouds are destroyed) are illustrated in a simple “contour” form in Figure 5. We find that all clouds in this regime can be at least order-of-magnitude described by traditional cloud-crushing arguments (Klein et al. 1994). This conclusion holds regardless of the specific physics included in a given simulation (e.g., conduction, or self gravity), with the classical cloud-crushing estimate $t_{\text{cc}} \sim \chi^{1/2} R_{\text{cl}}/v_{\text{cl}}$ providing a reasonable qualitative starting point to understand the actual cloud destruction times in the simulations. The majority of this section is dedicated to explaining why this is the case.

Before discussing physics, it is helpful to analyze our full simulation set to understand how the cloud lifetime varies with different parameters. Given the non-scale-free nature of the physical effects we include, there is not an obvious set of dimensionless parameters with which to fit the data, so we opt to simply use the physical parameters L_{cl} , n_{h} , T_{h} , and v_{cl} . Figure 6 shows that how the cloud lifetimes, normalized by classical cloud-destruction time t_{cc} , scale with each of these four parameters. We perform a multi-variable log-linear fitting to these four parameters, and find that predicted

lifetime scales as approximately,

$$t_{\text{life, pred}} \approx 10 t_{\text{cc}} \tilde{f} \quad (19)$$

$$\tilde{f} \equiv (0.9 \pm 0.1) L_1^{0.3} n_{0.01}^{0.3} T_6^{0.0} v_{100}^{0.6}$$

where $L_1 \equiv L_{\text{cl}}/1 \text{ pc}$ and $n_{0.01} \equiv n_{\text{h}}/0.01 \text{ cm}^{-3}$. The $1\text{-}\sigma$ values of the power-law dependences on $[L_{\text{cl}}, n_{\text{h}}, T_{\text{h}}, v_{\text{cl}}]$ are $[0.3 \pm 0.1, 0.3 \pm 0.1, 0.0 \pm 0.1, 0.6 \pm 0.1]$. This fit is plotted in Figure 7. For clouds with $v_{\text{h}} > 10 \text{ km s}^{-1}$, and for clouds in a cooler ambient medium with $T_{\text{h}} = 10^5 \text{ K}$, the dependence of $t_{\text{life, pred}}/t_{\text{cc}}$ on v_{h} is much weaker. This is discussed further in §3.5.3 below.

Given the complex and non-scale-free physics involved in our default simulations, the fit (Eq. 19) is remarkably universal. In particular, it is rather surprising that by simply assuming a separable power law in each variable, we have almost directly reproduced the classical cloud-crushing time, aside from the small correction factor \tilde{f} . We now discuss the reason for this universality by discussing in turn the effects that different physics have on the cloud-crushing process. These effects are shown graphically in Figure 8, showing a cloud in the process of being crushed, as we successively add physics to the pure hydrodynamical simulation (far left) in the form of (from left to right) cooling, magnetic fields, conduction, viscosity, self-shielding, and self-gravity.

3.5.1 Effect of Radiative Cooling

Radiative cooling has a modestly significant effect on cloud lifetime, as discussed in previous works (see, e.g., Section 5.3 of Klein et al. 1994). The basic effect of cooling on gas is to soften its equation of state (lower γ), which effectively renders the cloud more compressible (Scannapieco & Brüggén 2015). This makes the cloud more strongly crushed in the direction transverse to the flow, forming a thinner, denser filament with a smaller cross section. Although KH instabilities can grow more violently on this thinner cloud than for an adiabatic cloud because it moves faster with respect to the hot medium (due to its smaller drag), the net effect is for the cloud to survive modestly longer than an equivalent cloud with no cooling due to its higher density. This behavior is nicely illustrated by the comparison of the black and blue curves in Figure 9. Moreover, as shown in the left two panels of Figure 8, cooling can also enhance the formation of smaller, denser cloudlets in the wake (McCourt et al. 2018). This effect, however, can be suppressed by magnetic fields (Figure 8, see also Grønnow et al. 2018). Detailed analyses of the cloudlet properties have been carried out in several recent works (e.g., Sparre et al. 2019).

3.5.2 Effect of Magnetic Fields

Magnetic fields can modify cloud destruction in two qualitatively distinct ways: (1) dynamically (via magnetic pressure or tension), or (2) by suppressing conduction/viscosity.

Regarding (1), the magnetized “cloud-crushing” problem without cooling, conduction, or viscosity is well-studied (see Mac Low et al. 1994; Jones et al. 1996; Shin et al. 2008, and references therein); for very strong fields within or surrounding the cloud such that magnetic pressure is comparable to ram pressure (i.e., $P_{\text{B}} \gtrsim P_{\text{ram}} \sim \rho v_{\text{cl}}^2$, or $\beta \lesssim \mathcal{M}_{\text{h}}^{-2}$), cloud destruction is strongly suppressed. While $\beta \lesssim 1$ is common in very cold (e.g., molecular) gas in the ISM, in the warm and hot CGM realistic estimates of β range from $\sim 10^2 - 10^9$ (see Su et al. 2017; Martín-Alvarez et al. 2018; Hopkins et al. 2019), viz., the direct dynamical effects of the fields are negligible. Alternatively, it has been proposed that a strong field could build up via “magnetic draping” (Markevitch & Vikhlinin 2007), wherein the cloud “sweeps up” field lines oriented perpendicular to v_{cl} , compressing the field leading the cloud and increasing

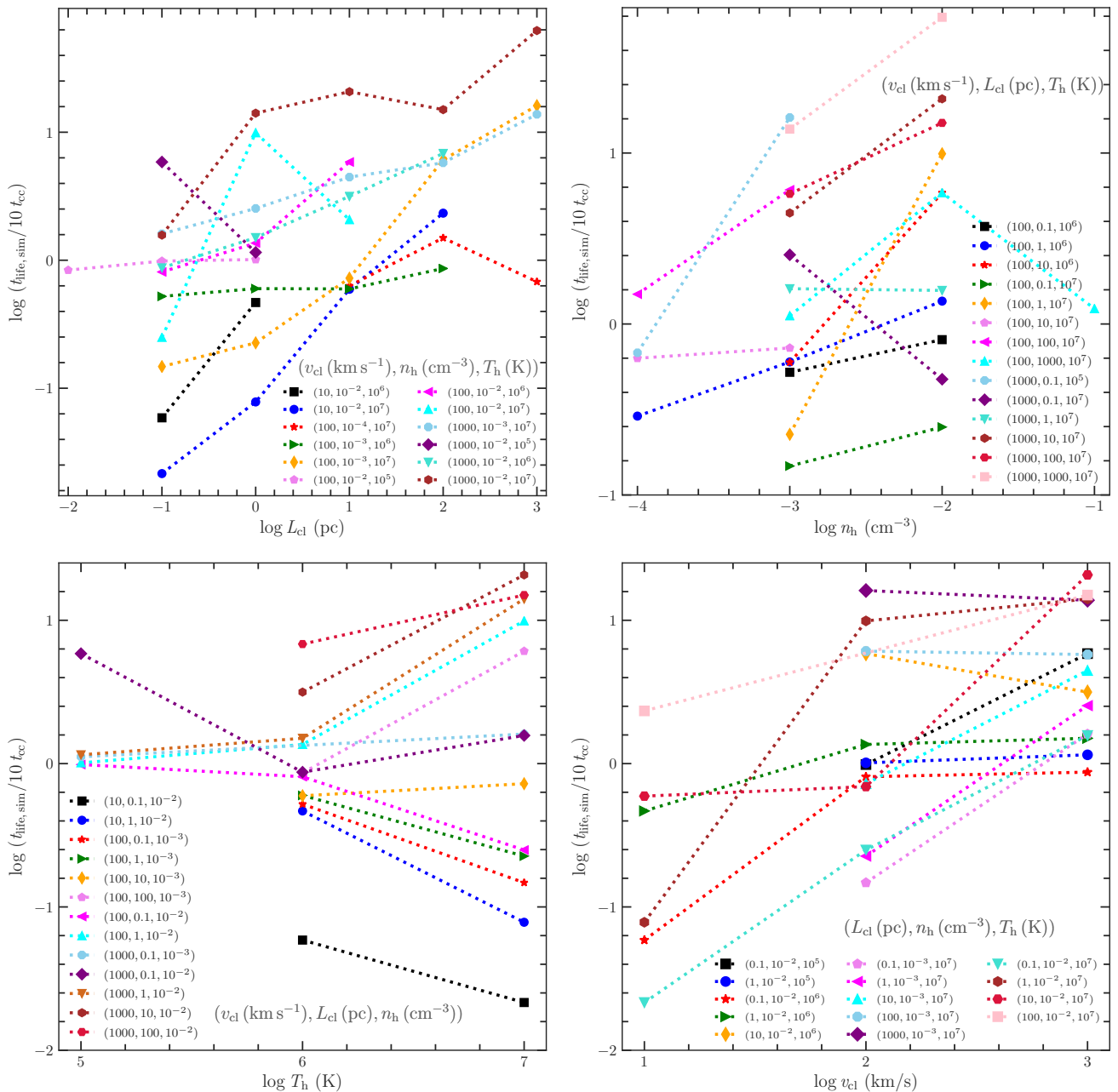


Figure 6. Simulated cloud “lifetimes”, $t_{\text{life, sim}}$ (in units of ten cloud-crushing time, $10 t_{\text{cc}}$) v.s. different initial conditions: cloud size L_{cl} , ambient density n_{h} , ambient temperature T_{h} and cloud velocity v_{cl} . Dotted lines connect simulations that have one varying parameter but otherwise identical initial conditions. In units of t_{cc} , the cloud lifetime has a weak dependence on T_{h} , modestly increases with L_{cl} and n_{h} (i.e., cloud N_{H}), and a slightly stronger dependence on v_{cl} . These dependencies are captured in the scaling of $t_{\text{life, pred}}$ with \tilde{f} in Eq. 19. Note that we factor out t_{cc} because it is the dominant effect here: our most extreme cases differ by factors of $\sim 10^8$ in their absolute lifetimes or values of t_{cc} (see e.g., Figure 3); the “residuals” here, while still large (~ 1 dex), are much smaller.

[B]. Miniati et al. (1999) define the “draping time,¹⁰” which we can turn into the equivalent length:

$$L_{\text{drape}} \sim \frac{\pi R_{\text{cl}} \chi^{2/3}}{50} \left(\frac{P_{\text{ram}} + P_{\text{therm}}}{P_{\text{B}}} \right)^{2/3} \approx 3 \text{ kpc } R_{\text{pc}} (\beta_{1000} T_6 v_{100}^2)^{2/3} \quad (20)$$

L_{drape} is the path length that a cloud must travel for the accumu-

¹⁰ We emphasize that the context in which draping was originally proposed referred to much larger structures, namely “bubbles” and jets emanating from AGN in the CGM of massive halos/clusters, which have physical size scales $\sim 10 - 100 \text{ kpc}$ and travel $\gtrsim 100 \text{ kpc}$, vastly different from what we model here.

lated field to appreciably alter its destruction (assuming $P_{\text{therm}} \ll P_{\text{ram}}$ for supersonic clouds). However, L_{drape} is much longer than the length scale over which clouds are destroyed, $L_{\text{cc}} \approx t_{\text{cc}} v_{\text{cl}} \approx 9 \text{ pc } R_{\text{pc}} v_{100} \mathcal{M}_{\text{cl}}^{-1}$. In other words, CGM magnetic fields are nowhere near sufficiently strong to dynamically suppress cloud destruction. This can be seen visually by comparing the second and third panels of Figure 8 (or the relevant lines in Figure 9), which shows how MHD and hydrodynamic simulations remain very similar without the effects of conduction. We have also confirmed this conclusion by re-running a subset of our simulations with plasma β multiplied or divided by a factor of ~ 1000 , which makes no difference to the

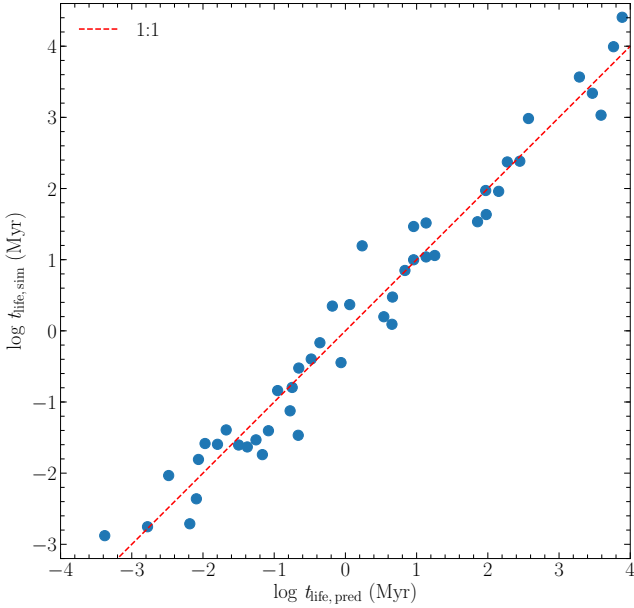


Figure 7. Cloud lifetimes measured in simulations ($t_{\text{lifc, sim}}$) versus the “predicted” lifetimes ($t_{\text{lifc, pred}}$) from a simple multi-variable power-law fit to t_{lifc} versus L_{cl} , n_{h} , T_{h} , and v_{cl} , given in Eq. (19). Given a dynamic range $\sim 10^8$ in absolute cloud lifetimes, the simulations can be remarkably well-fit by a power law of the form $t_{\text{lifc, pred}} \approx 10 t_{\text{cc}} \tilde{f}$ with $\tilde{f} \sim L_{\text{cl}}^{0.3} n_{\text{cl}}^{0.3} v_{\text{cl}}^{0.6}$ (so \tilde{f} encompasses all deviations from the cloud-crushing scaling).

measured lifetimes (as expected, since they remain in the weak-field limit).

However, regarding (2), even a very weak field is sufficient to suppress perpendicular conduction, viscosity (typically the perpendicular transport coefficients are suppressed by $\sim \lambda_{e, \text{gyro}}/\lambda_{e, \text{h}} \sim 10^{-8}$) and hydrodynamic instabilities (Dursi & Pfrommer 2008; Banda-Barragán et al. 2016, 2018). In this case the field geometry is what matters, while the field strength is irrelevant. In Figure 10, we therefore explore a series of simulations of one of our typical cloud-destruction cases, varying the initial field geometry. In general, the magnetic field configuration does not have a strong effect on the evolution of cloud mass. This is not surprising, as draping can rearrange the geometry of the magnetic field around the cloud to similar configurations and yield similar amount of suppression of conduction, viscosity and instabilities, regardless of the initial field geometry (note that the arguments of §3.5.3 below suggest that conduction plays only a secondary role anyway). However, in several extreme cases, such as when the magnetic field is aligned with the relative velocity ($\mathbf{B} \parallel \mathbf{v}_{\text{cl}}$), we do see a more rapid decrease in the cloud mass as there is essentially no draping. In contrast, with an azimuthal field configuration (looped magnetic fields inside the cloud plus $\mathbf{B} \perp \mathbf{v}_{\text{cl}}$ outside the cloud), the cloud mass decreases most slowly, indicating that the field can shield the cloud particularly efficiently in this case¹¹(see also Li et al. 2013; Banda-Barragán et al. 2016; Grønnow et al. 2017).

3.5.3 Effect of Conduction

The influence of conduction on isolated, undisturbed clouds (i.e., those without an impinging wind) has been studied by Cowie

¹¹ Note that in the “cloud growing” regime, transverse magnetic fields can shield the cloud via draping, reduce both mixing and warm gas mass loading and prevent condensation (see Grønnow et al. 2018). Also note that self-contained magnetic fields can enhance clumping and reduce cloud destruction (Li et al. 2013; McCourt et al. 2015; Banda-Barragán et al. 2018). We defer a detailed study of these effects to future work.

& McKee (1977b); McKee & Cowie (1977); Balbus & McKee (1982). For the range of temperatures relevant to our study ($10^5 \text{ K} \lesssim T_{\text{h}} \lesssim 10^7 \text{ K}$) the conclusion of these papers is that cloud evaporation/condensation is controlled by the saturation parameter¹²

$$\sigma_0 \approx 3.2 \frac{\lambda_{e, \text{h}}}{R_{\text{cl}}} \approx 0.4 \frac{T_6^3}{\langle n_{\text{cl}} \rangle R_{\text{pc}}} \approx T_6^3 \left(\frac{N_{\text{H}}}{1.2 \times 10^{18} \text{ cm}^{-2}} \right)^{-1} \quad (21)$$

For small values of $\sigma_0 \lesssim 0.01$ (large clouds), the cooling of the hot material onto the cloud is sufficiently rapid that the cloud condenses. The necessary size of such clouds ($N_{\text{H}} \gtrsim 1.2 \times 10^{20} \text{ T}_6^3 \text{ cm}^{-2}$) corresponds, within an order of magnitude, to the “growing-cloud” regimes discussed in §3.2–§3.4 (the cloud sizes required for growth in the crushed problem are slightly larger, which intuitively makes sense given they are being actively ripped apart by the wind). On the other side, large values of $\sigma_0 \gtrsim \chi$ correspond to the smallest clouds discussed in §3.1, which are immediately evaporated by hot electrons penetrating throughout the entire cloud (Balbus & McKee 1982). Thus, effectively all of our clouds in the “classical cloud destruction” regime lie in the range $0.01 \lesssim \sigma_0 \lesssim \chi$, which, in the absence of the hot wind would slowly evaporate into the ambient medium. As shown by McKee & Cowie (1977), the conductive heat flux that evaporates the cloud is in the unsaturated regime for clouds with $\sigma_0 \lesssim 1$, while the heat flux is saturated for $\sigma_0 \gtrsim 1$.

To make further progress, let us compare the cloud evaporation timescale to the cloud-crushing time. In the $\sigma_0 \lesssim 1$ regime, Cowie & McKee (1977b) compute the mass-loss rate by solving the hydrodynamic equations in spherical geometry, deriving the evaporation time of the cloud as (setting $\ln \Lambda_D = 30$)

$$t_{\text{evap}} \approx 30 \text{ Myr} n_{0.01} R_{\text{pc}}^2 T_6^{-5/2} \quad (22)$$

In the $\sigma_0 \gtrsim 1$ regime, where the heat flux is saturated, one can derive the evaporation time by comparing the rate at which energy is transferred to the cold cloud due to the saturated heat flux,

$$\dot{E} = 4\pi R_{\text{cl}}^2 q_{\text{sat}} \approx 4\pi \alpha R_{\text{cl}}^2 n_{\text{h}} c_{s, e, \text{h}} k_B T_{\text{h}} \quad (23)$$

(here $\alpha \approx 0.3$ is chosen to match Eq. 9), to the total energy required to evaporate the cloud by heating it up to the hot-medium temperature,

$$E \approx \frac{4}{3} \pi R_{\text{cl}}^3 n_{\text{cl}} k_B T_{\text{h}} \quad (24)$$

(A more complicated approach in Cowie & McKee (1977b) gives a similar estimate; see their Eq. 64). Because the heat flux is effectively given by the minimum of the unsaturated and saturated values (see Eq. 9), the time for the cloud to evaporate is the maximum of the unsaturated and saturated estimates, or

$$\frac{t_{\text{evap}}}{t_{\text{cc}}} \approx \max \left\{ 2 \mathcal{M}_{\text{h}} n_{\text{cl}} L_{\text{pc}} T_6^{-5/2}, 0.3 \mathcal{M}_{\text{h}} T_6^{1/2} \right\} \quad (25)$$

Note that the saturated (right-hand) expression is simply $\approx v_{\text{cl}}/(300 \text{ km s}^{-1})$.

We see that across the range of parameters surveyed, $t_{\text{evap}}/t_{\text{cc}}$ ranges from much larger than 1 for large clouds in fast winds, to somewhat less than 1 for smaller clouds. What will be the effect of this evaporation on the cloud-crushing process? For $t_{\text{evap}}/t_{\text{cc}} \ll 1$ we expect the cloud to behave effectively as it would in the absence of a wind, evaporating rapidly into the hot medium. On the other hand, when $t_{\text{evap}}/t_{\text{cc}} \gtrsim 1$ the evaporation has only a minor effect on the cloud lifetime, because it is crushed by the wind before

¹² We define σ_0 to match the numerical value given of σ_0 in McKee & Cowie (1977), which leads to a slightly different definition in terms of $\lambda_{e, \text{h}}/R_{\text{cl}}$ compared to Cowie & McKee (1977b) because of a different definition of $\lambda_{e, \text{h}}$.

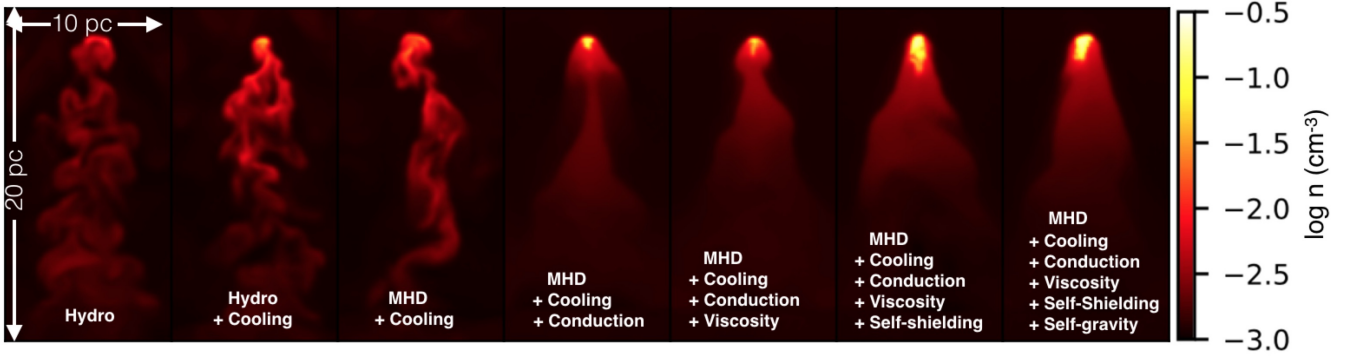


Figure 8. Sliced density maps for a cloud in the “classical cloud destruction” regime ($T_h = 10^6$ K, $v_{cl} = 100$ km s $^{-1}$, $n_h = 10^{-3}$ cm $^{-3}$, $L_{cl} = 1$ pc), with each panel from left to right showing a simulation that includes additional physical effects (at the same physical time, 0.3 Myr). From left to right we show: Hydro = ideal hydrodynamics; Hydro + Cooling = ideal hydrodynamics + radiative cooling, etc. Our default physics set is MHD + Cooling + Conduction + Viscosity. The cloud mass evolution curves for the same set of simulations are shown in Figure 9.

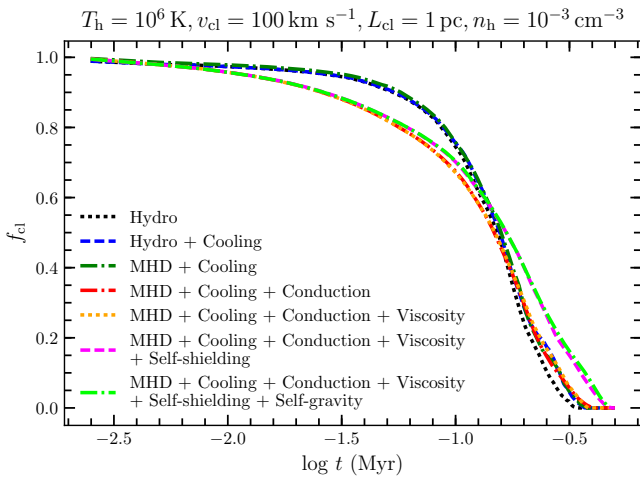


Figure 9. Evolution of the normalized cloud mass, f_{cl} (defined in Figure 1) versus time, for the simulations shown in Figure 8 ($T_h = 10^6$ K, $v_{cl} = 100$ km s $^{-1}$, $n_h = 10^{-3}$ cm $^{-3}$, $L_{cl} = 1$ pc) with different physics included (labeled as in Figure 8). The cloud mass versus time is remarkably similar across these runs, given the different physics and morphologies in Figure 8.

the heat flux has much of an effect (the static approach of Cowie & McKee 1977b also becomes highly questionable in such a strongly perturbed cloud). There does, however, seem to be a reasonably significant effect on the cloud morphology, which is evident in the change between the third and fourth panels of Figure 8 (see also Brüggén & Scannapieco 2016). This type of behavior, which occurs at $t_{evap}/t_{cc} \sim 1$, seems to be related to the fast creation of a conductive boundary layer, which causes an inwards pressure on the cloud due to the outflow of hot material from its outer edges. This compresses the cloud and increases its density, which sometimes has the effect of modestly increasing the cloud lifetime. Indeed, if we make the gross approximation that the mass is lost from the cloud with an outflow velocity that is approximately the ion sound speed (since the ions will be heated by the impinging hot electrons to approximately T_h), one finds that the ratio of the inwards pressure due to the outflow ($P_{evap} \approx \dot{m} v_{out}/(4\pi R^2) \approx m v_{out}/(4\pi R^2 t_{evap})$) to the thermal pressure of the cloud (P_{cl}) is approximately

$$\frac{P_{evap}}{P_{cl}} \approx \min \left\{ 2 \frac{T_6^3}{n_{cl} R_{pc}}, 10 \right\} \quad (26)$$

where the left-hand expression is that of the unsaturated ($\sigma_0 \lesssim 1$) regime, and the right-hand expression is that of the saturated ($\sigma_0 \gtrsim 1$) regime. We thus see that for smaller clouds, the pressure from

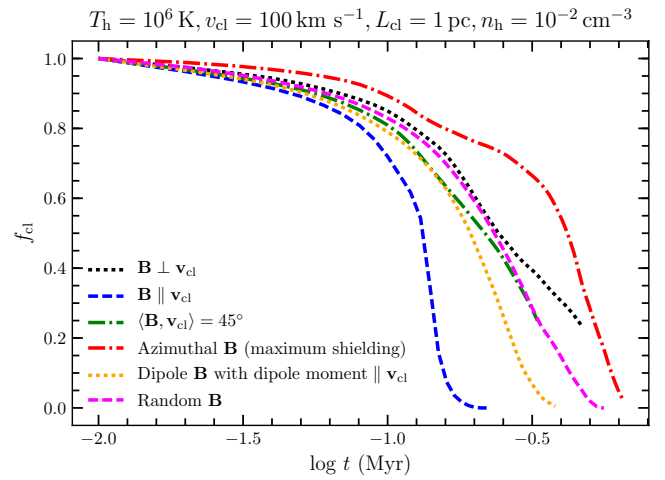


Figure 10. Evolution of the normalized cloud mass, f_{cl} (defined in Figure 1) versus time, for otherwise identical initial conditions ($T_h = 10^6$ K, $v_{cl} = 100$ km s $^{-1}$, $n_h = 10^{-2}$ cm $^{-3}$, $L_{cl} = 1$ pc) with different magnetic field configurations. We can see that when the magnetic field is aligned with the relative velocity ($\mathbf{B} \parallel \mathbf{v}_{cl}$), the cloud mass decreases most rapidly. For the azimuthal configuration (looped magnetic fields inside the cloud plus $\mathbf{B} \perp \mathbf{v}_{cl}$ outside the cloud, which produces maximal shielding to conduction), the cloud mass decreases most slowly. In all other cases, the magnetic field configuration does not have a large effect on the mass evolution: the lifetimes are identical to within a factor of < 2 .

evaporative outflow is modestly large compared to that of the cloud, and should thus be able to cause some compression, as seen in Figure 8.

The broad ideas of the previous paragraphs are confirmed in Figure 11, which plots t_{life}/t_{cc} v.s. σ_0 for our full suite of simulations, with each point colored by t_{evap}/t_{cc} from Eq. 25. We see that, as expected, only those simulations with $t_{evap}/t_{cc} \ll 1$ are destroyed significantly faster than t_{cc} (these are all low-velocity clouds). The lifetime of simulations with $t_{evap}/t_{cc} \gtrsim 1$ is mostly independent of σ_0 , aside from a possible slight increase in lifetime for $\sigma_0 \gtrsim 1$, which may be indicative of cloud compression due to the evaporative outflow. Finally, we note that this general framework explains our measured empirical scaling of t_{life}/t_{cc} with a positive power of v_{cl} (see Eq. 19), because the lowest velocity clouds are quickly destroyed by saturated conduction, i.e., their $t_{life} \sim t_{evap} \propto t_{cc} v_{cl}$ (Eq. 25), while those with higher velocities can live somewhat longer than t_{cc} due to the evaporative compression to higher densities. Meanwhile, for e.g., $T_h = 10^5$ K, all clouds fall into the $\sigma_0 \lesssim 1$

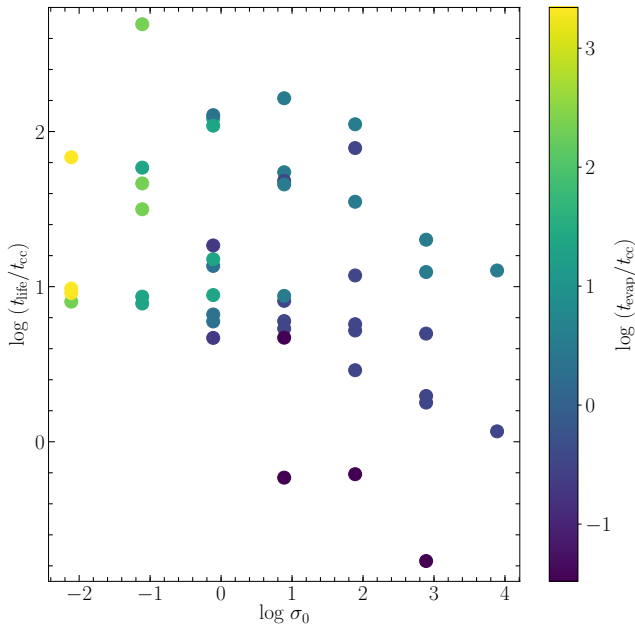


Figure 11. The simulated cloud lifetimes in units of the cloud-crushing time, $t_{\text{life}}/t_{\text{cc}}$, v.s. the saturation parameter, σ_0 (Eq. 21 in § 3.5.3, which quantifies the strength of conduction) for clouds in the “classical destruction” regime. The simulations are color-coded from light yellow to dark blue with decreasing $t_{\text{evap}}/t_{\text{cc}}$, where t_{evap} is the cloud evaporation time for a non-moving cloud in a conducting medium (Eq. 25). Simulations with $t_{\text{evap}} \ll t_{\text{cc}}$ are evaporated before cloud-crushing, explaining why $t_{\text{life}} \ll t_{\text{cc}}$. These clouds almost exclusively have $\sigma_0 \gg 1$, i.e., are in the regime of saturated conduction, where $t_{\text{evap}} \propto t_{\text{cc}} v_{\text{cl}}$, explaining the strong dependence of \tilde{f} on v_{cl} . While for simulations with $t_{\text{evap}} \gg t_{\text{cc}}$, clouds are only weakly influenced by conduction, and therefore $t_{\text{life}} \propto t_{\text{cc}}$.

regime (see Eq. 21), where $t_{\text{evap}}/t_{\text{cc}} > 1$ and the evaporative pressure (Eq. 26) is unimportant, so we simply obtain $t_{\text{life}} \propto t_{\text{cc}}$.

3.5.4 Effect of Viscosity

The effect of viscosity is in general sub-dominant to conduction. This is not surprising because conduction is controlled by the thermal velocity of hot electrons, while viscosity is controlled by the thermal velocity of ions, and the ratio of these thermal velocities (and thus the strength of conductivity and viscosity) is $(m_i/m_e)^{1/2} \sim 40$, assuming each has the same temperature. Nonetheless, viscosity does provide some non-zero insulating effects as a viscous “boundary layer” that forms around the cloud, which drags the co-moving boundary layer and can slightly increase the cloud lifetime for some clouds. This minor effect can be seen through the comparison of the fourth and fifth panels in Figure 8.

3.5.5 Effect of Turbulence in the Cloud or Ambient Medium

Some historical studies have argued that clouds which have initial “turbulence” (large density and velocity fluctuations) like GMCs in the ISM (e.g., Schneider & Robertson 2015, and references therein) might be much more rapidly-disrupted. However, most of these studies have considered clouds with large internal turbulent Mach numbers $\mathcal{M}_{\text{cl}}^{\text{turb}} \equiv |\delta \mathbf{v}_{\text{turb}}|/c_{s,\text{cl}} \sim 10 - 100$, akin to GMCs (see § 1), e.g., Schneider & Robertson (2015) consider an internal 3D Mach number $\mathcal{M}_{\text{cl}}^{\text{turb}} \sim 9$ (or equivalently, 1D Mach number $\mathcal{M}_{\text{cl}}^{\text{turb}} \sim 5$), which produces nearly ~ 1 dex initial rms density fluctuations.

However, for realistic turbulent Mach numbers in the CGM, turbulence should produce much weaker effects. This is because the initial cloud temperature is 10^4 K ($c_{s,\text{cl}} = 10 \text{ km s}^{-1}$), as compared to ~ 10 K in GMCs, and the density and temperature fluc-

tuations only become very large for large turbulent Mach numbers ($\mathcal{M}_{\text{cl}}^{\text{turb}} \gg 1$), which are highly unrealistic in the CGM (e.g., clouds do not have internal velocity dispersions of $\sim 100 \text{ km s}^{-1}$). The turbulent Mach numbers should be even lower in the hot medium. Moreover, $\mathcal{M}_{\text{cl}}^{\text{turb}} \gg 1$ is not a self-consistent “cloud” under the conditions we consider, because it necessarily implies a turbulent ram pressure much larger than the confining gas pressure (the “cloud” would simply fly apart as soon as the simulation begins): in GMCs this is resolved by confinement via self-gravity, but we have already excluded this regime.

We therefore have considered a subset of simulations using initial conditions drawn from driven periodic box simulations of turbulence (taken from Colbrook et al. 2017), for the cloud itself, the ambient hot medium, or both, with Mach numbers in each medium of $\sim 0.1, 0.5, 1$. Not surprisingly, these have little effect on the supersonic cloud-crushing process (consistent with Banda-Barragán et al. 2018, 2019). For example, for $\mathcal{M}_{\text{cl}} \sim 0.1$, the initial density and pressure fluctuations are only of the order of $\sim 1\%$, much smaller than those introduced almost immediately by the cloud-wind interaction. We therefore do not discuss these cases in more detail.

4 CONCLUSIONS

In this paper, we have systematically explored the survival of cool clouds traveling through hot gas – the so-called “cloud crushing” problem – for parameters relevant to the CGM. We present a comprehensive parameter survey, with cloud diameters from $\sim 0.01 - 1000 \text{ pc}$, relative velocities $\sim 10 - 1000 \text{ km s}^{-1}$, ambient temperatures $\sim 10^5 - 10^7$ K and ambient densities $\sim 10^{-4} - 10^{-1} \text{ cm}^{-3}$. We study the effects of a range of physics, including radiative cooling, anisotropic conduction and viscosity, magnetic fields, self-shielding and self-gravity. We identify several unique regimes, which give rise to qualitatively different behaviors, including collapse, growth, expansion, shredding, and evaporation. For mid-sized clouds, those in the “classical cloud destruction” regime, we also quantify the cloud lifetime as a function of parameters across the broad range of initial conditions. We reach a number of important conclusions, including:

(i) Clouds which are *initially* self-gravitating/J Jeans-unstable, or self-shielding to molecular/low-temperature metal-line fine-structure cooling and thus able to cool to temperatures $T \ll 1000$ K, will fragment and form stars before they are disrupted. For clouds that are initially Jeans-stable and non-shielding, these effects can be neglected. This transition occurs when the cloud exceeds large, DLA-like column densities (Eq. 14, 15).

(ii) In an ambient medium where the “diffuse” gas cooling time is shorter than the time for diffuse gas to cross the cloud ($\sim R_{\text{cl}}/v_{\text{cl}}$), pressure-confinement of the cloud cannot effectively operate and the cloud-crushing problem is ill-posed. In hotter medium ($T_{\text{h}} \gtrsim 10^6$ K) this only occurs at high enough column densities such that the cloud would already be self-gravitating; while in cooler ambient halos ($T_{\text{h}} < 10^6$ K), which are generally not able to sustain a “hot halo” in quasi-hydrostatic equilibrium, even clouds with more modest column densities $N_{\text{H}} \gtrsim 10^{18} \text{ cm}^{-2}$ can reach this regime (see Eq. 16).

(iii) If the expected destruction time of a cloud through shocks and fluid mixing (cloud crushing) is longer than the cooling time of the swept-up material in the shock front leading the cloud, the cloud can grow in time, rather than disrupt (Gronke & Oh 2018). The cooling of the shock front material adds to the cloud mass (with the growth time simply being the timescale to “sweep up” new mass), faster than instabilities can disrupt the cloud, and the cloud acts more like a seed for the thermal instability. This can occur at column densities well below the self-gravity/shielding/ambient medium rapid cooling thresholds above (see Eq. 17).

(iv) If we restrict to clouds *below* the sizes/column densities of the above thresholds, and *above* the size/column density where they become smaller than the penetration length of hot electrons into the cloud ($N_{\text{H}} \gtrsim 10^{16} \text{ cm}^{-2} T_6^2$; Eq. 13), then we find that the clouds are indeed disrupted and mixed by a combination of instabilities, shocks, and conduction. Remarkably, the cloud lifetimes can be well fit by a single power law similar to the classical “cloud-crushing” scaling for the pure hydrodynamic problem, albeit with a larger normalization and a secondary dependence on the ambient temperature and velocity, which is introduced by the combination of cooling and conduction. We develop simple analytic scalings to understand how this modification to the scaling arises.

(v) Braginskii viscosity, turbulent density/velocity fluctuations in the cloud, and magnetic field geometry and strength have relatively weak effects on cloud lifetimes and do not qualitatively alter our conclusions. Viscous effects tend to be sub-dominant to conduction because of the relative scaling of ion and electron mean-free-paths in the CGM (although we caution that our model assumes equal ion and electron temperatures). Turbulent effects are weak for realistic initial cloud turbulence, because CGM clouds, unlike GMCs in the ISM, cannot be highly supersonic (this would require *internal* turbulent Mach numbers in the cloud $\gg 1$). This implies that the initial density fluctuations in the cloud are quite small. Magnetic field strength has little effect because the CGM plasma has $\beta \gg 1$ (i.e., magnetic pressure is much weaker than thermal pressure, which is yet smaller than the ram pressure) and the distance clouds would have to travel to acquire dynamically important fields via “draping” is much longer than the length over which they are destroyed. Field geometry has some effect, by suppressing thermal conduction in the directions perpendicular to the field. However, we show the net effect of the field geometry is minor for most plausible geometries ($\sim 10\%$ in t_{life}) and even the most extreme favorable/unfavorable field geometries produce only a factor of ~ 2 systematic change in cloud lifetimes.

We caution that there are still a number of caveats to this study. There remain a number of simplifications in the physics included in our model (Eqs. 2–7), which may be important for some regimes. The most important of these is likely the assumption of equal electron and ion temperatures, even in the presence of strong conduction and cooling on scales approaching the electron mean free path. Indeed, because the timescale for ions to collisionally equilibrate with electrons is $\sim m_i/m_e$ times the electron-electron collision timescale, regions with large (saturated) electron heat fluxes may also have $T_e \gg T_i$ or $T_i \gg T_e$. Unfortunately, tackling this issue in detail is difficult and computationally demanding even in simplified setups (see, e.g., Kawazura et al. 2019), and is well beyond current computational capabilities for a highly inhomogeneous problem such as cloud crushing. On fluid scales, there are also significant uncertainties that arise from our basic numerical setup, which we have intentionally restricted to be rather idealized. Potential complications that might be relevant and interesting to study in future work include lack of pressure equilibrium in the cool gas (as could arise from, e.g., supersonic turbulence, Banda-Barragán et al. 2018), the effect of stratification of the ambient medium, and the interaction with scales that are not resolved in our simulations here (see, e.g., McCourt et al. 2018). However, in view of the simple physical arguments that have supplemented most of the main conclusions of this paper (see above), it seems unlikely that these effects would cause significant qualitative changes to our main results.

ACKNOWLEDGMENTS

Support for ZL and co-authors was provided by an Alfred P. Sloan Research Fellowship, NSF Collaborative Research Grant #1715847

and CAREER grant #1455342, and NASA grants NNX15AT06G, JPL 1589742, 17-ATP17-0214. JS acknowledges the support of the Royal Society Te Apārangi through a Rutherford Discovery Fellowship RDF-U001804 and Marsden Fund grant UOO1727. Numerical calculations were run on the Caltech compute cluster “Wheeler;” allocations from XSEDE TG-AST130039 and PRAC NSF.1713353 supported by the NSF, and NASA HEC SMD-16-7592.

REFERENCES

- Armillotta L., Fraternali F., Werk J. K., Prochaska J. X., Marinacci F., 2017, *MNRAS*, **470**, 114
- Balbus S. A., McKee C. F., 1982, *ApJ*, **252**, 529
- Banda-Barragán W. E., Parkin E. R., Federrath C., Crocker R. M., Bicknell G. V., 2016, *MNRAS*, **455**, 1309
- Banda-Barragán W. E., Federrath C., Crocker R. M., Bicknell G. V., 2018, *MNRAS*, **473**, 3454
- Banda-Barragán W. E., Zertuche F. J., Federrath C., García Del Valle J., Brügger M., Wagner A. Y., 2019, *MNRAS*, **486**, 4526
- Braginskii S. I., 1965, *Reviews of Plasma Physics*, **1**, 205
- Brügger M., Scannapieco E., 2016, *ApJ*, **822**, 31
- Cen R., 2013, *ApJ*, **770**, 139
- Chen H.-W., Lanzetta K. M., Webb J. K., Barcons X., 1998, *ApJ*, **498**, 77
- Churchill C. W., Steidel C. C., Vogt S. S., 1996, *ApJ*, **471**, 164
- Colbrook M. J., Ma X., Hopkins P. F., Squire J., 2017, *MNRAS*, **467**, 2421
- Cowie L. L., McKee C. F., 1977b, *ApJ*, **211**, 135
- Cowie L. L., McKee C. F., 1977a, *ApJ*, **211**, 135
- Dedner A., Kemm F., Kröner D., Munz C. D., Schnitzer T., Wesenberg M., 2002, *Journal of Computational Physics*, **175**, 645
- Dursi L. J., Frommer C., 2008, *ApJ*, **677**, 993
- Faucher-Giguère C.-A., Lidz A., Zaldarriaga M., Hernquist L., 2009, *ApJ*, **703**, 1416
- Faucher-Giguère C.-A., Hopkins P. F., Kereš D., Muratov A. L., Quataert E., Murray N., 2015, *MNRAS*, **449**, 987
- Federrath C., Banerjee S., 2015, *MNRAS*, **448**, 3297
- Ferland G. J., Korista K. T., Verner D. A., Ferguson J. W., Kingdon J. B., Verner E. M., 1998, *PASP*, **110**, 761
- Gronke M., Oh S. P., 2018, *MNRAS*, **480**, L111
- Gronke M., Oh S. P., 2019, *MNRAS*, **p. 2995**
- Grønnow A., Tepper-García T., Bland -Hawthorn J., McClure-Griffiths N. M., 2017, *ApJ*, **845**, 69
- Grønnow A., Tepper-García T., Bland -Hawthorn J., 2018, *ApJ*, **865**, 64
- Hopkins P. F., 2015, *MNRAS*, **450**, 53
- Hopkins P. F., 2016, *MNRAS*, **462**, 576
- Hopkins P. F., 2017, *MNRAS*, **466**, 3387
- Hopkins P. F., Raives M. J., 2016, *MNRAS*, **455**, 51
- Hopkins P. F., et al., 2018, *MNRAS*, **480**, 800
- Hopkins P. F., et al., 2019, *MNRAS*, **p. 2993**
- Johnson S. D., Chen H.-W., Mulchaey J. S., Schaye J., Straka L. A., 2017, *ApJ*, **850**, L10
- Jones T. W., Ryu D., Tregillis I. L., 1996, *ApJ*, **473**, 365
- Kawazura Y., Barnes M., Schekochihin A. A., 2019, *Proceedings of the National Academy of Science*, **116**, 771
- Kereš D., Hernquist L., 2009, *ApJ*, **700**, L1
- Klein R. I., McKee C. F., Colella P., 1994, *ApJ*, **420**, 213
- Komarov S. V., Churazov E. M., Kunz M. W., Schekochihin A. A., 2016, *MNRAS*, **460**, 467
- Körtgen B., Federrath C., Banerjee R., 2019, *MNRAS*, **482**, 5233
- Krumholz M. R., Gnedin N. Y., 2011, *ApJ*, **729**, 36
- Kulsrud R. M., 1983, in Sagdeev R. N., Rosenbluth M. N., eds., *Handbook of Plasma Physics*. Princeton University
- Kunz M. W., Schekochihin A. A., Stone J. M., 2014, *Phys. Rev. Lett.*, **112**, 205003
- Li S., Frank A., Blackman E. G., 2013, *ApJ*, **774**, 133
- Li S., Frank A., Blackman E. G., 2014, *MNRAS*, **444**, 2884
- Liang C. J., Remming I. S., 2018, arXiv e-prints, [p. arXiv:1806.10688](https://arxiv.org/abs/1806.10688)
- Liang C. J., Kravtsov A. V., Agertz O., 2016, *MNRAS*, **458**, 1164
- Mac Low M.-M., McKee C. F., Klein R. I., Stone J. M., Norman M. L., 1994, *ApJ*, **433**, 757
- Markevitch M., Vikhlinin A., 2007, *Phys. Rep.*, **443**, 1

- Martin-Alvarez S., Devriendt J., Slyz A., Teyssier R., 2018, *MNRAS*, 479, 3343
- McCourt M., O’Leary R. M., Madigan A.-M., Quataert E., 2015, *MNRAS*, 449, 2
- McCourt M., Oh S. P., O’Leary R., Madigan A.-M., 2018, *MNRAS*, 473, 5407
- McKee C. F., Cowie L. L., 1975, *ApJ*, 195, 715
- McKee C. F., Cowie L. L., 1977, *ApJ*, 215, 213
- Miniati F., Jones T. W., Ryu D., 1999, *ApJ*, 517, 242
- Mouschovias T. C., 1976a, *ApJ*, 206, 753
- Mouschovias T. C., 1976b, *ApJ*, 207, 141
- Orr M. E., et al., 2018, *MNRAS*, 478, 3653
- Price D. J., Monaghan J. J., 2007, *MNRAS*, 374, 1347
- Prochaska J. X., Lau M. W., Hennawi J. F., 2014, *ApJ*, 796, 140
- Rahmati A., Pawlik A. H., Raičević M., Schaye J., 2013, *MNRAS*, 430, 2427
- Richter P., Paerels F. B. S., Kaastra J. S., 2008, *Space Sci. Rev.*, 134, 25
- Robertson B. E., Kravtsov A. V., 2008, *ApJ*, 680, 1083
- Sarazin C. L., 1988, X-ray emission from clusters of galaxies
- Savage B. D., Lehner N., Narayanan A., 2011, *ApJ*, 743, 180
- Scannapieco E., Brügggen M., 2015, *ApJ*, 805, 158
- Schneider E. E., Robertson B. E., 2015, *ApJS*, 217, 24
- Shin M.-S., Stone J. M., Snyder G. F., 2008, *ApJ*, 680, 336
- Sparre M., Pfrommer C., Vogelsberger M., 2019, *MNRAS*, 482, 5401
- Spitzer L., Härm R., 1953, *Physical Review*, 89, 977
- Springel V., 2005, *MNRAS*, 364, 1105
- Squire J., Schekochihin A. A., Quataert E., Kunz M. W., 2019, *Journal of Plasma Physics*, 85, 905850114
- Steidel C. C., Erb D. K., Shapley A. E., Pettini M., Reddy N., Bogosavljević M., Rudie G. C., Rakic O., 2010, *ApJ*, 717, 289
- Stocke J. T., Penton S. V., Danforth C. W., Shull J. M., Tumlinson J., McLin K. M., 2006, *ApJ*, 641, 217
- Su K.-Y., Hopkins P. F., Hayward C. C., Faucher-Giguère C.-A., Kereš D., Ma X., Robles V. H., 2017, *MNRAS*, 471, 144
- Thompson T. A., Quataert E., Zhang D., Weinberg D. H., 2016, *MNRAS*, 455, 1830
- Tumlinson J., Peebles M. S., Werk J. K., 2017, *ARA&A*, 55, 389
- Werk J. K., et al., 2014, *ApJ*, 792, 8
- Werk J. K., et al., 2016, *ApJ*, 833, 54
- Yao Y., Wang Q. D., Penton S. V., Tripp T. M., Shull J. M., Stocke J. T., 2010, *ApJ*, 716, 1514

APPENDIX A: CONVERGENCE TESTS

We have verified that our results are robust to numerical resolution ($m_i \sim 10^{-7} - 10^{-3} M_{\text{cl}}$, or equivalently, $\sim 134 - 6$ cells per R_{cl}) via a variety of tests. For at least one cloud in every “regime” shown in Figure 5, we have re-run the same initial conditions at three resolution levels (our default, and one and two orders-of-magnitude lower resolution). In all cases we confirm that the measured cloud lifetime is robust to better than a factor of ~ 2 (although the cloud lifetimes do become systematically shorter at low resolution, as expected owing to numerical mixing). We have also randomly selected ten clouds in the “classical cloud destruction” regime to simulate at both lower and higher resolutions (a factor of ~ 8 change): we find the lifetimes change by a factor of < 1.5 in these cases. In Figure A1, we show one fiducial cloud, for which we simulate at seven different resolution levels. The agreement in cloud lifetime is excellent at order-of-magnitude higher and lower resolutions, compared to our default choice in the main text, which lends confidence to our conclusion that our key results are not strongly sensitive to numerical resolution.

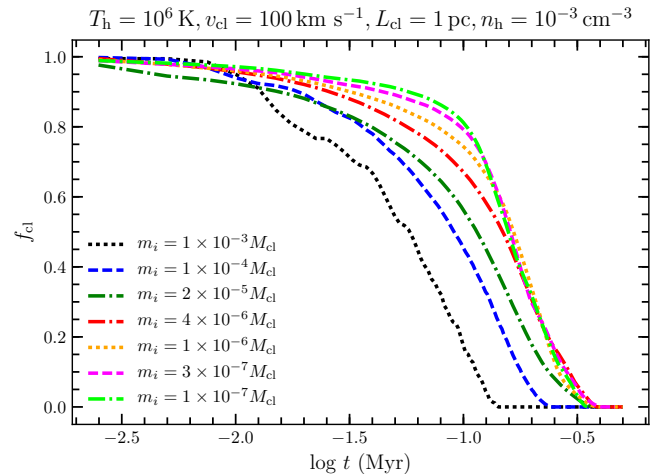


Figure A1. Evolution of the normalized cloud mass, f_{cl} (defined in Figure 1) versus time, for one representative initial condition in the “classical cloud destruction” regime ($T_h = 10^6 \text{ K}$, $v_{\text{cl}} = 100 \text{ km s}^{-1}$, $n_h = 10^{-3} \text{ cm}^{-3}$, $L_{\text{cl}} = 1 \text{ pc}$) with our default physics set simulated at seven different mass resolution (m_i) levels, as labeled. The resulting cloud lifetime is remarkably robust to resolution, changing by $< 10\%$ from $m_i/M_{\text{cl}} \sim 10^{-5} - 10^{-7}$ and by a factor of < 2 (< 3) even at resolutions $m_i/M_{\text{cl}} \sim 10^{-4}$ ($\sim 10^{-3}$). Recall our default resolution in the main text is $m_i/M_{\text{cl}} \sim 10^{-6}$. The small change in behavior at early times and high resolution (with a longer “delay” until destruction begins) owes to better tracking of small, high-density “features” (e.g. Kelvin-Helmholtz whorls) which remain locally high density even as mixing begins.